Cell Systems

Article

Clonal differences underlie variable responses to sequential and prolonged treatment

Highlights

- Melanoma clones were traced through multiple rounds of treatment
- Cells within clones maintain gene expression similarities over 2 months of treatment
- Different clones have distinct fates during continued treatment
- Initial treatment can cause changes in sensitivity to secondary treatment

Authors

Dylan L. Schaff, Aria J. Fasse, Phoebe E. White, Robert J. Vander Velde, Sydney M. Shaffer

Correspondence

sydshaffer@gmail.com

In brief

Schaff et al. show that resistant cancer cell clones are different from one another, yet the cells within a clone remain similar during treatment. They also show that transcriptional differences between clones result in different cell fates when treated sequentially with different agents or continuously with the same agent.

Schaff et al., 2024, Cell Systems *15*, 213–226
March 20, 2024
https://doi.org/10.1016/j.cels.2024.01.011

CellPress

Cell Systems

CellPress

Article

Clonal differences underlie variable responses to sequential and prolonged treatment

Dylan L. Schaff,[1,5] Aria J. Fasse,[2,4,5] Phoebe E. White,[2] Robert J. Vander Velde,[1,3] and Sydney M. Shaffer[1,3,6,*]
[1]Department of Bioengineering, School of Engineering and Applied Sciences, University of Pennsylvania, Philadelphia, PA 19146, USA
[2]Department of Chemistry, School of Arts and Sciences, University of Pennsylvania, Philadelphia, PA 19146, USA
[3]Department of Pathology, Perelman School of Medicine, University of Pennsylvania, Philadelphia, PA 19146, USA
[4]Division of Biology and Biological Engineering, California Institute of Technology, Pasadena, CA 91125, USA
[5]These authors contributed equally
[6]Lead contact
*Correspondence: sydshaffer@gmail.com
https://doi.org/10.1016/j.cels.2024.01.011

SUMMARY

Cancer cells exhibit dramatic differences in gene expression at the single-cell level, which can predict whether they become resistant to treatment. Treatment perpetuates this heterogeneity, resulting in a diversity of cell states among resistant clones. However, it remains unclear whether these differences lead to distinct responses when another treatment is applied or the same treatment is continued. In this study, we combined single-cell RNA sequencing with barcoding to track resistant clones through prolonged and sequential treatments. We found that cells within the same clone have similar gene expression states after multiple rounds of treatment. Moreover, we demonstrated that individual clones have distinct and differing fates, including growth, survival, or death, when subjected to a second treatment or when the first treatment is continued. By identifying gene expression states that predict clone survival, this work provides a foundation for selecting optimal therapies that target the most aggressive resistant clones within a tumor. A record of this paper's transparent peer review process is included in the supplemental information.

INTRODUCTION

Individual cancer cells frequently exhibit diverse responses to their environment and to treatments, resulting in some cells surviving while others die. These surviving cells can contribute to the development of treatment-resistant tumors, limiting the effectiveness of treatment. Although genetic differences often account for these varied responses,[1–3] non-genetic factors,[4] such as epigenetic state,[5,6] protein levels,[7] gene expression,[8–11] and cell-cycle stage,[12] can also contribute to therapy resistance and survival in a hypoxic microenvironment.[13,14] Upon treatment, a subset of cancer cells survive and generate clones that are resistant to therapy. These resistant clones can exhibit high interclonal heterogeneity, characterized by divergent gene expression states and invasive properties.[9] However, it remains uncertain how these heterogeneous resistant clones respond when subjected to a second treatment.

Second-line treatments are typically less effective compared with first-line treatments.[15–18] However, it is unclear how this occurs at the level of resistant clones or individual cells. Specifically, it is unknown whether all resistant clones respond uniformly to a second treatment or whether they exhibit different responses (Figure 1A). Furthermore, when resistant clones undergo prolonged treatment with the same agent, it is unknown whether some clones grow more than others. While it is evident that treatment can drive clones into diverse resistant states,[9] their phenotypic consequences have yet to be revealed.

To address this gap, we developed an experimental and computational pipeline for long-term tracking of cancer cell clones through sequential and prolonged treatments. We employed DNA barcoding in melanoma cells and used both genomic DNA (gDNA) and single-cell RNA-sequencing (scRNA-seq) to monitor transcriptional and clonal changes over time. We separately applied a panel of three treatments, allowed 4 weeks for the development of resistant clones, and then divided samples so that cells from each resistant clone were separately treated again with each of the three treatments. This approach allowed for the same clones to be profiled through all combinations of treatments and treatment orders. Applying this technique, we found that clones exhibit divergent responses to the second treatment. Furthermore, cells within a resistant clone maintain their transcriptional similarity throughout both prolonged treatment with a single agent and sequential treatment with multiple agents. Finally, we demonstrated that gene expression differences between clones underlie a clone's ability to survive sequential and prolonged treatment.

RESULTS

Melanoma cell clones exhibit variable responses to a first and second treatment

To study cancer cell responses through sequential treatments, we selected three agents relevant to melanoma cells that have diverse mechanisms of action: (1) combined treatment with

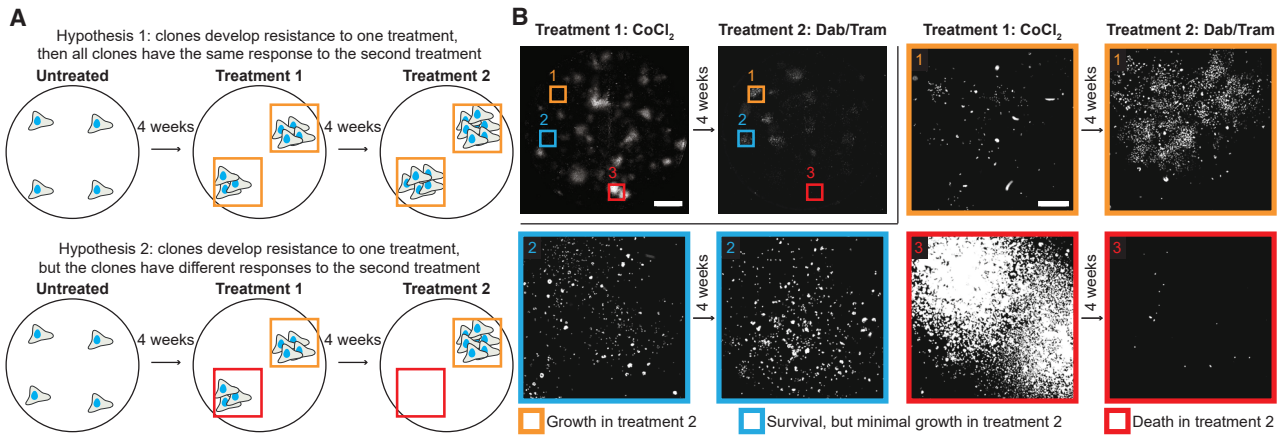

Figure 1. Melanoma cell clones exhibit variable responses to a first and second treatment

(A) Shown are two possible scenarios for how clones could respond to sequential treatment with different agents. All resistant clones derived from one treatment could have the same response to a second treatment (top), or they could have different responses to a second treatment (bottom).

(B) WM989 BRAF V600E mutant melanoma cells with a nuclear GFP tag imaged after 4 weeks in $CoCl_2$ followed by 4 weeks in combination dabrafenib and trametinib (Dab/Tram, top left). The top left images show whole-well scans of the clones. The colored boxes show zoomed images selected from the whole well. Orange shows a clone that grew in the second treatment, blue shows a clone that remained a similar size in the second treatment, and red shows a clone that died in the second treatment. $CoCl_2$-resistant cells tend to grow on top of each other causing some cropped images to look out of focus. Scale bars in whole-well scans represent 5 mm, while scale bars in cropped scans represent 500 μm and apply to all cropped scans.

dabrafenib[19] and trametinib,[20] which are targeted inhibitors of V600E mutant BRAF and MEK, respectively, (2) $CoCl_2$, which mimics hypoxia by activating many of the same stress responses,[21,22] and (3) the chemotherapeutic cisplatin, which kills cells by cross-linking DNA and inhibiting DNA replication.[23] We first investigated whether all clones that develop resistance to one of these treatments exhibit the same response to a second treatment. To visualize individual clones, we sparsely plated BRAF V600E mutant WM989 melanoma cells with a nuclear GFP tag and treated with either dabrafenib and trametinib in combination, $CoCl_2$, or cisplatin for 4 weeks. These treatments resulted in resistant clones that were easily resolved by imaging (Figures 1B and S1). We then applied a different treatment from our panel to these cells for another 4 weeks. We found that the individual resistant clones originating from the first treatment exhibited diverse responses to the second treatment, consistent with our second hypothesis in Figure 1A. By examining all the clones on the plate, we found that individual clones either grew, survived with minimal growth, or died in a second treatment (Figures 1B and S1). Thus, we concluded that resistant clones originating from one treatment could display highly variable responses to a second treatment. This finding motivated our study of resistant clones at the single-cell level to understand why some survive while others die with sequential treatments.

To build on our initial observation that resistant clones showed variable responses to a second treatment, we sought to generalize this result across a large number of clones and treatment conditions. We used cellular barcoding to allow us to track resistant clones across multiple treatments and through time.[9,11,24,25] We began by uniquely labeling individual cancer cells with a barcoding library developed by Emert et al.[26] (Figure 2A). We then allowed cells to undergo a limited number of divisions (~5.5 doublings; Table S2), producing numerous cells with the same barcode while preserving their gene expression similarities.[11,26] We performed barcode sequencing on a subset of cells to identify clones present before treatment and then divided the remaining population of cells three ways for separate initial treatments with either combination dabrafenib and trametinib, $CoCl_2$, or cisplatin. After 4 weeks of treatment, we performed scRNA-seq and barcode sequencing on a subset of surviving cells and replated the remaining cells from each treatment condition to receive a second round of treatment, with either the same or a different agent, continuing for 4 more weeks or until reaching confluency. We then repeated scRNA-seq and barcode sequencing of the surviving cells from the second round of treatment (Figure 2A). At each time point, we also sequenced the barcodes from the gDNA of a subset of cells to avoid undersampling the population-level clone dynamics by only including cells captured in the scRNA-seq (see STAR Methods). In summary, this experimental framework yielded quantitative tracking of the clones present before treatment, after the first treatment, and after the second treatment, as well as single-cell and clonally resolved transcriptomics of the resistant cells after the first and second treatments.

We first analyzed the gDNA barcode sequencing data to track clones before treatment and after each round of treatment. To equate our sequencing read data to a relative number of cells and set thresholds for resistant clones, we added a "ladder" of barcodes to each sample, consisting of defined numbers of cells with known barcodes (see STAR Methods). Using this ladder, we confirmed that sequencing reads increase with greater cell numbers (Figure S2A). Consequently, clones that are highly represented in the population will have a large number of sequencing reads, and those that are lowly represented will have few or no reads (Figure 2B).

Having established that barcode sequencing reads serves as a quantitative measurement of cell abundance, we next confirmed whether cells with the same barcode have similar responses to treatment. This behavior has been previously observed for BRAF inhibitors and MEK inhibitors in

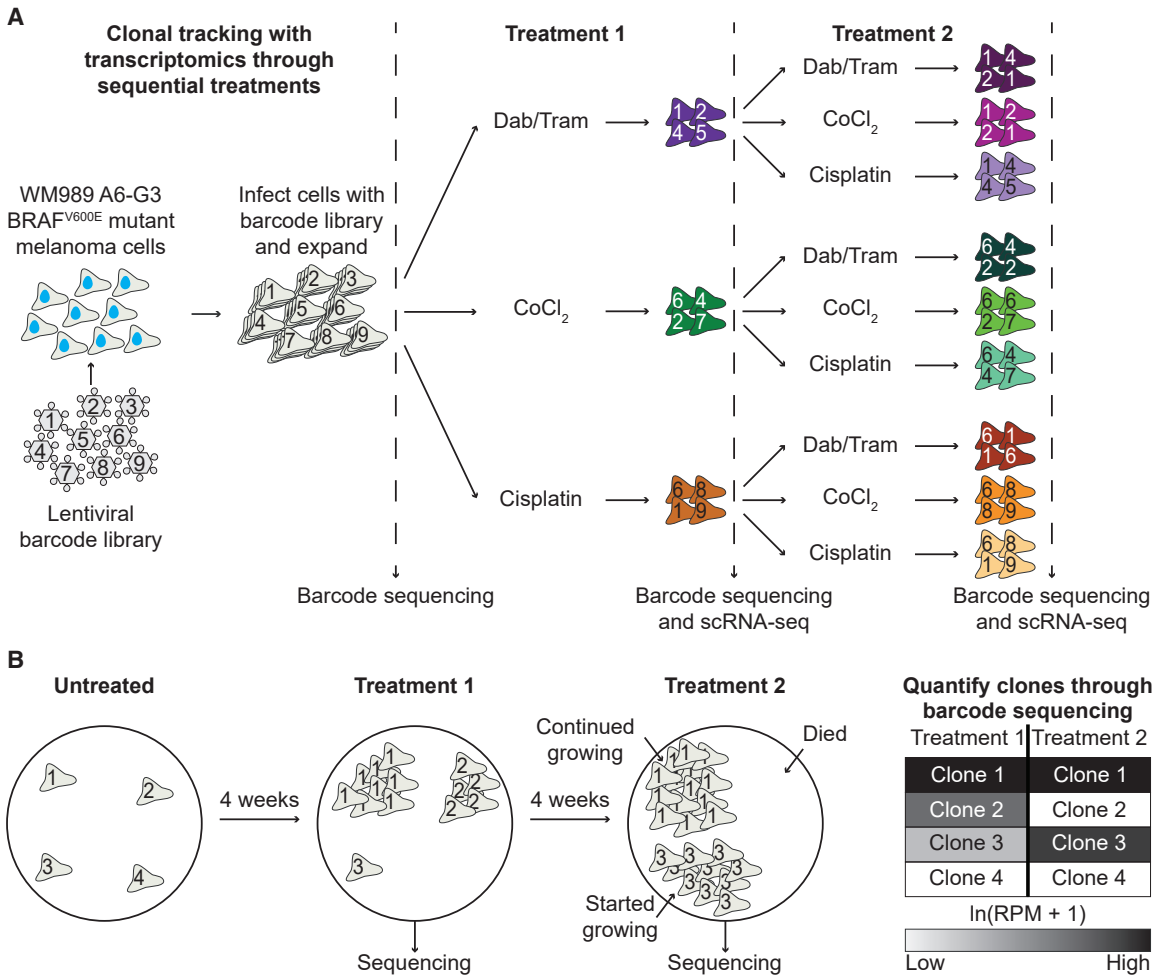

(legend on next page)

melanoma[9,26] and is critical for experiments using barcoding to track clones in resistance. Thus, we tested whether the resistance mechanisms to all agents in our study are heritable through cell division using a barcoding strategy adapted from prior work.[9,26] Using the same library as above, we transduced WM989 melanoma cells with barcodes, allowed them to grow through ~6 doublings, and then split them into separate samples for treatment, with two samples receiving each treatment. We extracted gDNA and sequenced the barcodes to assess for clone abundance in the separate samples. We found high correlation in barcode abundance between replicates for dabrafenib (Figure S2B), trametinib (Figure S2C), $CoCl_2$ (Figure S2D), and cisplatin (Figure S2E). We therefore concluded that the resistance phenotypes from these treatments are mediated by heritable processes that are largely preserved across cells through ~6 divisions.

We next asked whether clonal growth differences before treatment could explain growth through the first treatment (Figure S2F). We found that some of the largest clones in the untreated samples were also the largest clones after treatment with each agent. However, for each treatment, we also observed clones with low prevalence in the untreated sample, but high prevalence after the first round of treatment. Thus, initial growth differences in untreated clones are not sufficient to explain treatment outcomes.

When we compared the abundance of individual clones between the first and second treatments, we observed three distinct phenomena, which are schematically depicted in Figure 2B. First, we observed clones where the cells survived the first treatment while exhibiting minimal growth but then grew into large clones during the second treatment. Second, we observed clones that grew well during both the first and second treatment. Third, we also observed clones that grew well in the first treatment but then died and were absent after the second treatment. These results reinforce the notion that clonal differences in cells play an important role in response to a second treatment.

When comparing the clones captured after each of the first treatments, we detected a larger number of clones following cisplatin treatment than after combination treatment with dabrafenib and trametinib or $CoCl_2$ (Figures 2C and 2D). Furthermore, numerous clones with low abundance after initial treatment with dabrafenib and trametinib or $CoCl_2$ expanded when cisplatin was applied as the second treatment (Figure 2C). Although not entirely unique, secondary treatment with cisplatin selected for different clones than secondary treatment with dabrafenib and trametinib or with $CoCl_2$. Particularly notable in the case of cisplatin, we also saw that not all clones that survived the initial treatment were detected at the second time point with the same treatment. This result is surprising, as we would expect these clones to still be resistant at the second time point if they were resistant at the first. While it is possible that some clones are not remaining resistant through time, another possibility is that differences in growth rates between clones lead to different representations of the clones in the sequencing data. Particularly when we treat with cisplatin, we find that a few clones lose contact inhibition and grow very large (Figure S1). Colonies such as these could dominate the second time point and lead to less capture of small, yet still present clones. Broadly, these findings highlight the diverse clonal dynamics that can emerge with a single treatment and upon sequential treatments.

Treatment histories are remembered in gene expression states

Recent studies demonstrate that duration and dose of treatment can influence the transcriptional state of cancer cells.[8,9,27] Therefore, we asked whether the treatment history of multiple agents can be observed in the gene expression of surviving cells, and whether the first or second treatment has a greater effect on the final transcriptional state of a cell. We generated a uniform manifold approximation and projection (UMAP) of the final state of every cell that received two rounds of treatment (hypothetical data in Figure 3A; actual data Figure 3B). For each of the three treatments used, we then calculated the pairwise Pearson correlations in gene expression between cells that received the treatment first and compared them with the Pearson correlations of cells that received that treatment second (Figure 3B). To provide a baseline for comparison, we randomly sampled a group of the same number of cells from each condition and calculated a Pearson correlation among the random sample. Across every treatment, whether grouped by either the first or second therapy, the average pairwise Pearson correlation of gene expression similarity was at least ~3.5-fold higher than randomly grouped cells. We thus concluded that the final gene expression states of cells that received multiple treatments are influenced by both the first and second treatments.

We next compared the magnitude of the effects of the first and second treatments. We found that secondary treatment with dabrafenib and trametinib (~10.5-fold greater in average correlation) and cisplatin (~5-fold greater in average correlation) had a greater effect than initial treatment on gene expression as measured by the Pearson correlation coefficient (Figure 3B). However, we found the opposite result for cells treated with $CoCl_2$ (~2.5-fold less in average correlation). Therefore, cells receiving $CoCl_2$ as their first treatment were transcriptionally more similar than cells treated with $CoCl_2$ as a second treatment.

Figure 2. DNA barcoding allows for tracking the transcriptome of clones through multiple rounds of treatment

(A) Schematic showing experimental protocol for clone tracking and scRNA-seq of WM989 BRAF V600E mutant melanoma cells through treatment with dabrafenib and trametinib (Dab/Tram), $CoCl_2$, or cisplatin (see STAR Methods).

(B) Schematic showing how sequencing reads from the genomic DNA of cells that survived a treatment provide a quantitative readout of treatment response.

(C) Heatmaps showing 100 randomly subsampled and rank-ordered clones detected after initial treatment with Dab/Tram (left), $CoCl_2$ (middle), and cisplatin (right) followed by their abundance in the second round of treatment. Individual clones are colored by the ln(reads per million [RPM] + 1) using data from sequencing clonal barcodes from gDNA of surviving cells.

(D) The number of total detected clones per condition are displayed in their assigned color. It should be noted that there are clones whose abundance were below the threshold of detection after treatment 1 that were later detected in treatment 2. The total number of unique clones that were detected after the first or second treatment are displayed below each heatmap.

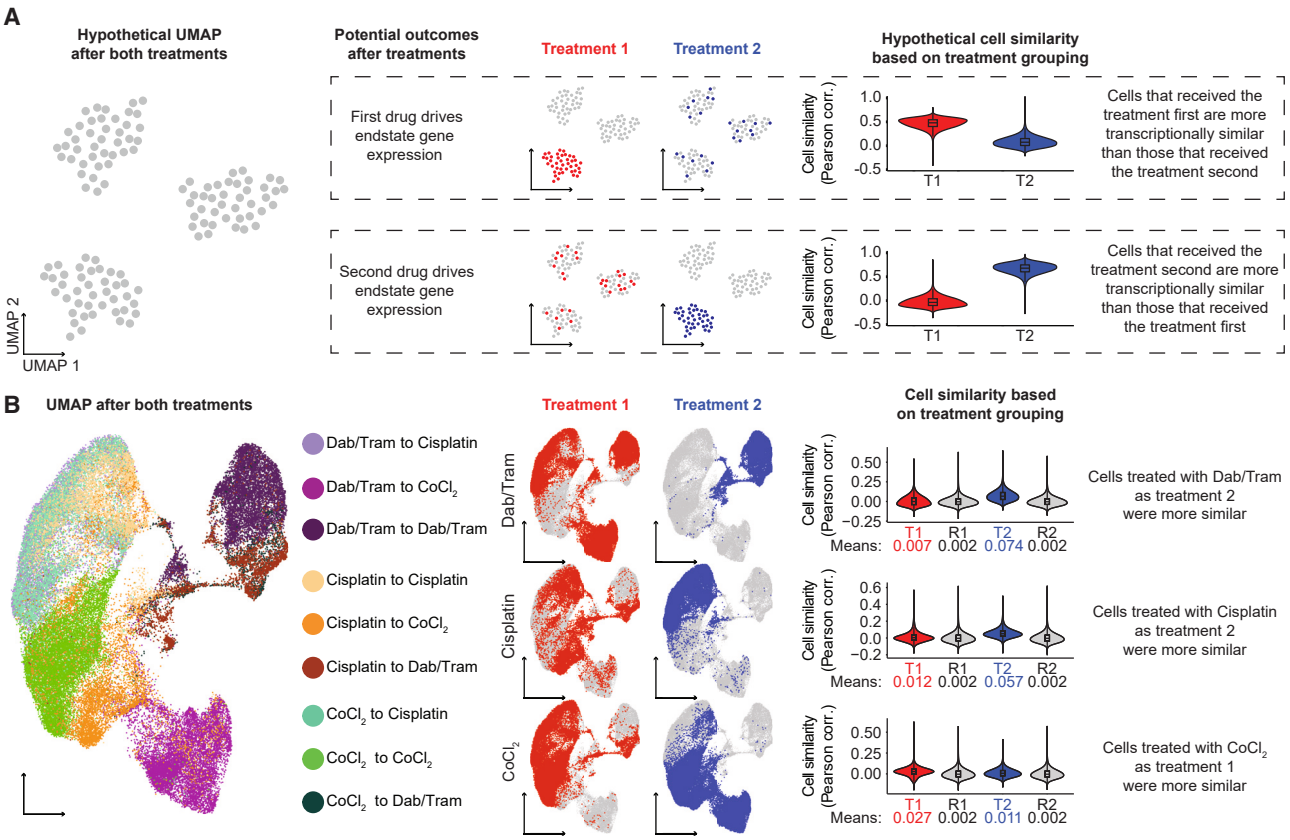

Figure 3. The treatment histories of cells are reflected in their gene expression

(A) Schematic showing the theoretical possibilities of the first treatment driving endstate gene expression (top) or the second treatment driving endstate gene expression (bottom). Displayed are how these possibilities would look in UMAP space or plotted as pairwise Pearson correlations between cell transcriptomes. (B) (Left) UMAP (GEO: GSE253739) of the nine conditions that had received both a first and second treatment. (Center) UMAP with cells that received the indicated treatment first highlighted in red and those that received the treatment second highlighted in blue. (Right) Quantification of cell similarity using pairwise Pearson correlations of gene expression (top 2,000 most variable genes). For combination dabrafenib and trametinib treatment (Dab/Tram), pairwise Pearson correlations between cells that received Dab/Tram first (treatment 1 [T1]) were ~3.5-fold higher than the matched random sampling of cells (random control 1 [R1]), while correlations between cells that received Dab/Tram second (treatment 2 [T2]) were ~37-fold higher than the matched control (random control 2 [R2]) and ~10.5-fold higher than those that received Dab/Tram first. For cisplatin treatment, pairwise Pearson correlations between cells that received cisplatin first were ~6-fold higher than the matched random sampling of cells, while correlations between cells that received cisplatin second were ~28.5-fold higher than the matched control and ~5-fold higher than those that received cisplatin first. For $CoCl_2$ treatment, pairwise Pearson correlations between cells that received $CoCl_2$ first were ~13.5-fold higher than the matched random sampling of cells and ~2.5-fold higher than those that received $CoCl_2$ second, while correlations between cells that received $CoCl_2$ second were ~5.5-fold greater than the matched random control. All comparisons were statistically significant by a two-sided t test with $p < 2.2e{-}16$. Violin plots display 10,000,000 subsampled data points per condition, but statistical comparisons and averages were calculated on non-subsampled data. Mean values are displayed below each graph.

None of these findings were affected when cells that received the same treatment twice were omitted (Figures S3A–S3C). These results collectively indicate that both the initial and subsequent treatments contribute to a cell's ultimate gene expression state, with the degree of influence varying depending on the treatment.

Despite treatment-induced changes in gene expression, cells within a clone remain transcriptionally similar to one another

Given that both the first and second treatments influence a cell's final gene expression state, we next wondered whether these treatment-induced changes effectively eliminated the intraclonal similarities in gene expression that have been previously described in multiple studies.[9,11,26] Thus, we analyzed the cells within each clone to assess if they retained transcriptional similarity after each treatment. For each sample, we identified resistant clones and calculated pairwise Pearson correlations between all cells within each clone (Figure 4A). We compared these pairwise correlations within clones to correlations calculated on 100 size-matched random samples of cells in the same treatment dataset (Figures S4A–S4L). For every condition, including those from the first treatment and the second treatment, the Pearson correlations within the clone were higher than the randomly sampled data (Figures 4B–4M). As expected, the correlations after prolonged treatment are predominantly lower than their associated 4-week sample. However, the pairwise Pearson correlations after the second treatment are still higher than those of randomly sampled cells. We also found that the level of transcriptional similarity is not strongly driven by the clone size, either before or after treatment (Figures S5A–S5O).

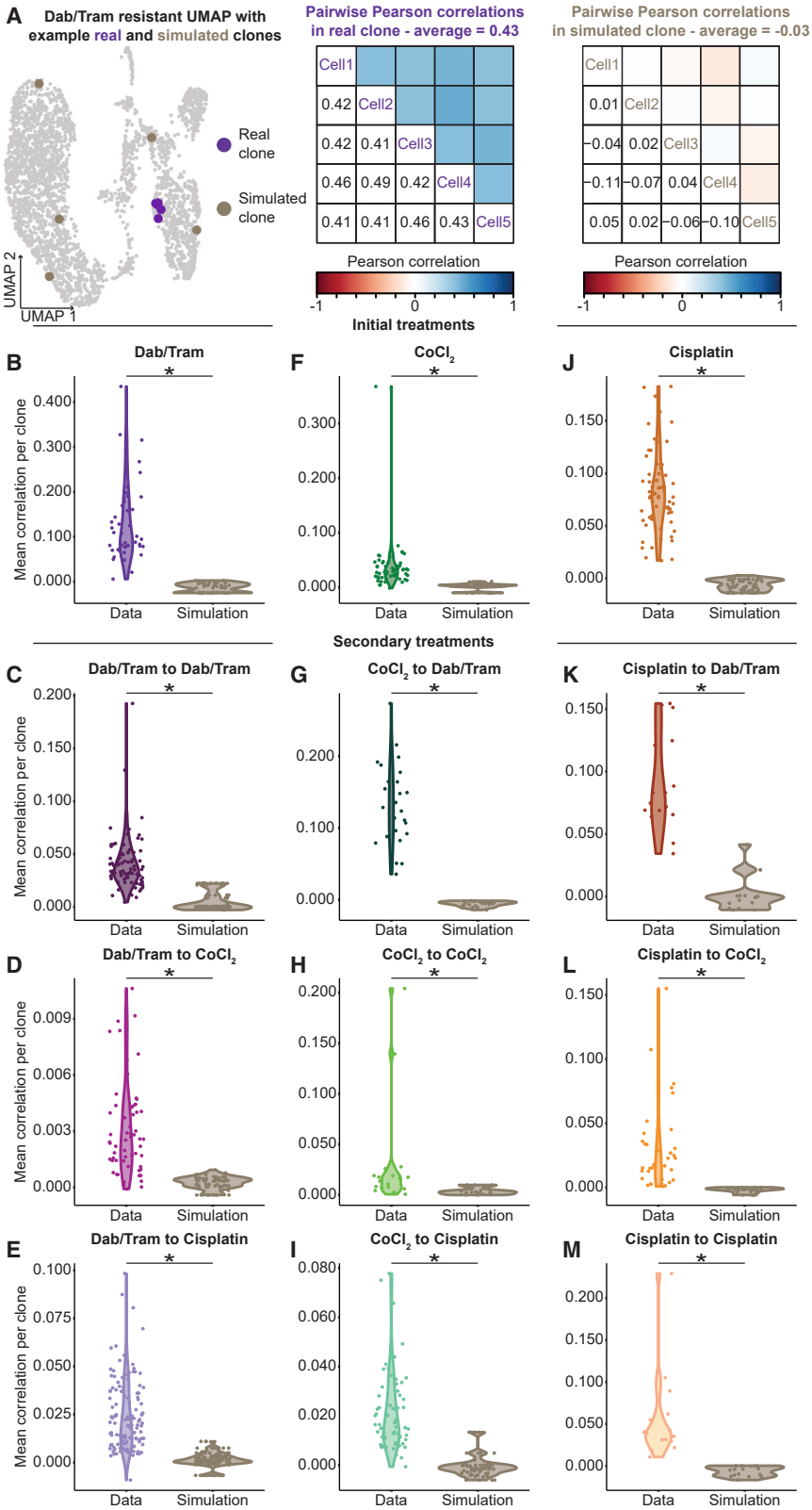

Figure 4. Cells within a clone maintain gene expression similarities through multiple rounds of treatment

(A) (Left) Location of the cells from a real clone (purple) and its matched random control (tan) from one simulation overlaid on the UMAP of dabrafenib- and trametinib-(Dab/Tram) resistant cells (GEO: GSE253739). (Middle) Pairwise Pearson correlations of gene expression (top 2,000 most variable genes) of cells from the real clone. The average of these pairwise Pearson correlations was 0.43. (Right) Pairwise Pearson correlations of gene expression of cells from the simulated clone. The average of these pairwise Pearson correlations was −0.03. For the pairwise Pearson correlation figures, the blocks above the diagonal are shaded according to the linear color scale to indicate the correlation, while the numerical value is displayed in the associated block in the lower diagonal. The averages of the pairwise Pearson correlations of the cells within each clone that received a treatment were compared with those of random samplings of the same number and sized clones over 100 simulations. Clones analyzed ranged from 5 to 11,257 cells. Displayed are the first simulations for each condition.

(B–M) As follows are the number of simulations where the observed similarities were higher than random for each condition by a one-sided Wilcoxon rank sum test with $p < 0.05$: (B) Dab/Tram 100/100, (C) Dab/Tram to Dab/Tram 100/100, (D) Dab/Tram to $CoCl_2$ 100/100, (E) Dab/Tram to cisplatin 100/100, (F) $CoCl_2$ 99/100, (G) $CoCl_2$ to Dab/Tram 100/100, (H) $CoCl_2$ to $CoCl_2$ 100/100, (I) $CoCl_2$ to cisplatin 100/100, (J) cisplatin 100/100, (K) cisplatin to Dab/Tram 100/100, (L) cisplatin to $CoCl_2$ 100/100, and (M) cisplatin to cisplatin 100/100.

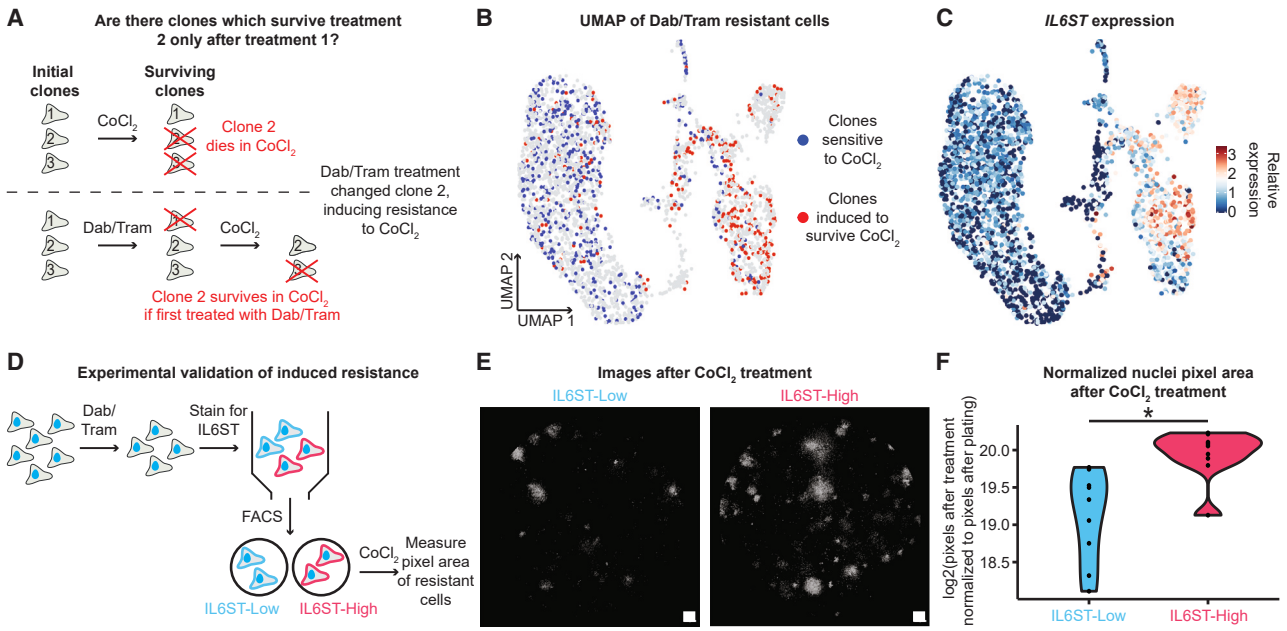

Figure 5. Treatment with dabrafenib and trametinib induces resistance to $CoCl_2$ in clones marked by high *IL6ST* expression

(A) Schematic showing how clone 2 only survived $CoCl_2$ treatment after being treated with dabrafenib and trametinib (Dab/Tram).

(B) UMAP (GEO: GSE253739) of dabrafenib- and trametinib-resistant cells. Cells from clones that will not survive (are sensitive to) $CoCl_2$ are colored blue, and cells from clones that were induced to survive $CoCl_2$ are colored in red (these did not survive $CoCl_2$ when applied as the first treatment).

(C) UMAP of dabrafenib- and trametinib-resistant cells showing relative expression of *IL6ST*. The color scale describes log-normalized data.

(D) Schematic for the validation of induced resistance. Cells were treated with dabrafenib and trametinib for 4 weeks. Dabrafenib- and trametinib- resistant cells were then stained for the expression of IL6ST protein and sorted into high (top 30%) and low (bottom 30%) populations. These IL6ST-high and -low populations were treated with $CoCl_2$ for an additional 4 weeks and then survival and growth was assessed by imaging.

(E) Representative DAPI images of IL6ST-low and -high dabrafenib- and trametinib-resistant cells after $CoCl_2$ treatment (one out of six analyzed whole-well images are displayed for each of the IL6ST-low and IL6ST-high conditions). We binarized the DAPI-stained nuclei images such that nuclei were white and the remaining pixels were black. Scale bars represent 2 mm.

(F) Violin plots showing the number of white pixels per well in IL6ST-low vs. -high cells. Each data point is a separate well from the experiment. These numbers were normalized to a plate that was scanned the day after plating to eliminate differences from seeding. $p < 5 \times 10^{-4}$ determined by a one-sided t test where the IL6ST-high cells were expected to have greater survival than the IL6ST-low cells. A second biological replicate is shown in Figure S6D.

Consequently, we concluded that cells within a clone remain transcriptionally similar to each other through sequential and prolonged treatment.

Some clones develop induced resistance with sequential treatment

Our experimental design, which started with a large pool of clones to test many sequential treatment combinations, provided a unique opportunity to identify clones that only survived a particular treatment after developing resistance to a different treatment beforehand—a phenomenon we termed "induced resistance" (Figure 5A). In each ordered combination of treatments, we identified hundreds of clones with induced resistance (Figures S6A, S6F, and S6G). To measure the gene expression differences in these induced resistant clones, we performed differential gene expression and gene set enrichment analysis comparing clones with induced resistance to clones that were sensitive to the second treatment (Figures S6A, S6C, and S6F–S6I). We discovered significant transcriptional and pathway-level differences in the induced resistant clones (Figures S6C, S6H, and S6I). One such pathway enriched in clones that only survived $CoCl_2$ after developing resistance to dabrafenib and trametinib was interleukin (IL)-6/JAK/STAT3 signaling (Figure S6C), of which IL6ST is an upstream cell-surface signaling transducer whose gene is also highly enriched[28] (Figures 5B and 5C). IL-6, which signals through IL6ST, has previously been implicated in chemotherapy and targeted inhibitor resistance in multiple cancer types.[29–32] We observed that *IL6ST* is infrequently expressed prior to treatment (expressed in 2.1% of cells; Figure S6B) but more frequently expressed after survival in dabrafenib and trametinib (expressed in 44.2% of the cells; Figure 5C). These findings suggest that treatment with dabrafenib and trametinib can cause otherwise $CoCl_2$-sensitive clones to become resistant, with this resistant state being marked by expression of *IL6ST*.

Given that dabrafenib- and trametinib-resistant cells are heterogeneous in their expression of *IL6ST*, we sought to experimentally validate that these *IL6ST*-high cells were indeed more resistant in $CoCl_2$. We first generated dabrafenib- and trametinib-resistant cells by treating them for 4 weeks. We then sorted these cells based on their expression of IL6ST protein and isolated the top 30% as IL6ST-high and the bottom 30% as IL6ST-low, selecting these cutoffs based roughly upon the heterogeneity observed in scRNA-seq. We then treated the sorted samples with $CoCl_2$ to test for differences in cell survival and growth (Figures 5D and 5E). We found that IL6ST-high samples

had more cells after treatment with $CoCl_2$ (Figures 5F, S6D, and S6E), thus confirming that IL6ST marks the dabrafenib- and trametinib-resistant subpopulation that is then more resistant to $CoCl_2$. Broadly, this supports our model in which resistance to one treatment can induce gene expression states that are correlated with resistance to another treatment.

Prolonged treatment with the same agent causes population-level and clonal changes in gene expression

We next investigated the gene expression changes in cells undergoing prolonged treatment with a single agent. We found that cells clustered based on the duration of treatment across our entire panel (Figure 6A). To assess pathway-level changes, we performed differential gene expression comparing samples at the first and second time points for each treatment. We then used enrichGO[33] to identify enriched pathways and grouped Gene Ontology (GO) terms that were related to similar cellular functions (Figures 6B and S7A–S7H). In all three treatments, we found that prolonged treatment resulted in significant changes in pathway activity, most of which have been reported in the literature to be involved with treatment resistance or aggressive cancer phenotypes.[34–41] Thus, across all three different treatments, we found further evidence that the transcriptional states of the population change dynamically as a function of the duration of treatment.[27]

Considering that treatment duration produced differences in transcriptional states, we identified two possible explanations for this observation. One possibility is that all clones undergo the same population-level changes in gene expression during treatment. Alternatively, individual clones might have heterogeneous changes during treatment, which collectively contribute to the average signal observed at the population level. To explore these possibilities, we performed the same pathway analysis at the clonal level (Figures 6C–6E). In targeted therapy with dabrafenib and trametinib, the majority of pathways that were differentially active between 4 and 6.5 weeks of treatment at the population level were not consistently differentially expressed on a clone-by-clone basis (Figure 6C). Similarly, pathways that were differentially active between cisplatin treated cells after 4 and 8 weeks at the population level were not reflected in most of the individual clones (Figure 6D), suggesting that clones can have differential responses to prolonged treatment with the same agent.

While the population-level changes with combination dabrafenib and trametinib or cisplatin were largely not evident in the majority of clones, we found that $CoCl_2$ showed the opposite result. Almost all $CoCl_2$ clones displayed the same pathway enrichment as the analysis performed at the population level (Figure 6E). Despite all of the clones going through similar gene and pathway expression changes, we still observed drastic changes in cell growth between clones, with one clone constituting 81% of the total cells sequenced after 8 weeks in $CoCl_2$. Across all three treatments, the one pathway where the population-level changes were reflected in all of the clones was cadherin binding, yet the directionality of this change varied across treatments. These findings demonstrate that different treatments can elicit different responses from individual clones.

We next asked whether these pathway differences also exist within the cells from a clone. We calculated pathway scores at the single-cell level using UCell[42] for each of the pathways analyzed above and verified that average changes in pathway expression by UCell followed the same trends in Figure 6B (Figure S8). We used these activity scores to analyze the variability both between clones (interclonal) and within clones (intraclonal) after first (Figures S9A and S9C) and second treatments (Figures S9B and S9D). Broadly, we observed that variability within the clones was greater than variability between the clones. Further, we found that certain pathways tended to have higher coefficients of variation than others and that high variability was most dependent on the pathway itself, rather than the treatment applied or the time point.

Clonal differences in gene expression underlie response to prolonged treatment with dabrafenib and trametinib

Given that individual clones can have different gene expression states after treatment, we next wondered whether the gene expression state of clones at the first time point could predict their outcome by the second time point in our experiment. Such a possibility would indicate that gene expression states of resistant cells could be valuable in predicting later behaviors of cells during the same or different treatments. For this analysis, we focused specifically on combination treatment with dabrafenib and trametinib. Previous works from our lab and others have shown that *EGFR*, *NGFR*, and other receptor tyrosine kinases are highly associated with intrinsic and adaptive resistance to dabrafenib and trametinib.[8,11,43–46] Our scRNA-seq data of dabrafenib- and trametinib-resistant cells from both time points showed two independent clusters of resistant cells, one which was high in *EGFR* and another which was high in *NGFR* (Figures S10A–S10D). We hypothesized that these divergent transcriptional states correlated with differences in survival to prolonged treatment with dabrafenib and trametinib. After 4 weeks of treatment with dabrafenib and trametinib, we identified 44 resistant clones, 23 of which were exclusively in the *EGFR*-high cluster, five of which were exclusively in the *NGFR*-high cluster, and 16 of which had cells in both clusters (Figure 7A). When comparing cells from clones in the *EGFR*- or *NGFR*-high clusters with melanoma differentiation states outlined by Tsoi et al.,[47] we found that the *EGFR*-high cells were the most ''undifferentiated,'' while the *NGFR*-high cells were the most ''melanocytic'' (Figures S10H–S10K).

We then followed these 44 clones through an additional 2.5 weeks in dabrafenib and trametinib. We found that 13.0% and 18.8% of the *EGFR*-high and mixed clones were no longer detected, respectively, (as defined by no longer passing resistant thresholds; see STAR Methods). However, 100% of the *NGFR*-high clones were not detected at this second time point (Figure 7A), suggesting that *EGFR*-high clones survive and proliferate better than *NGFR*-high clones. The disappearance of specific clones at the second time point could result from these clones dying during the extra weeks of treatment, or it might be due to *EGFR*-high clones proliferating faster and causing the *NGFR*-high clones to be not detected when subsampling for scRNA-seq. This result aligns with previous findings that melanoma cells exhibit a range of differentiation states,[47–49] where the more undifferentiated cells with higher receptor tyrosine kinase expression (as seen in the *EGFR*-high clones) are

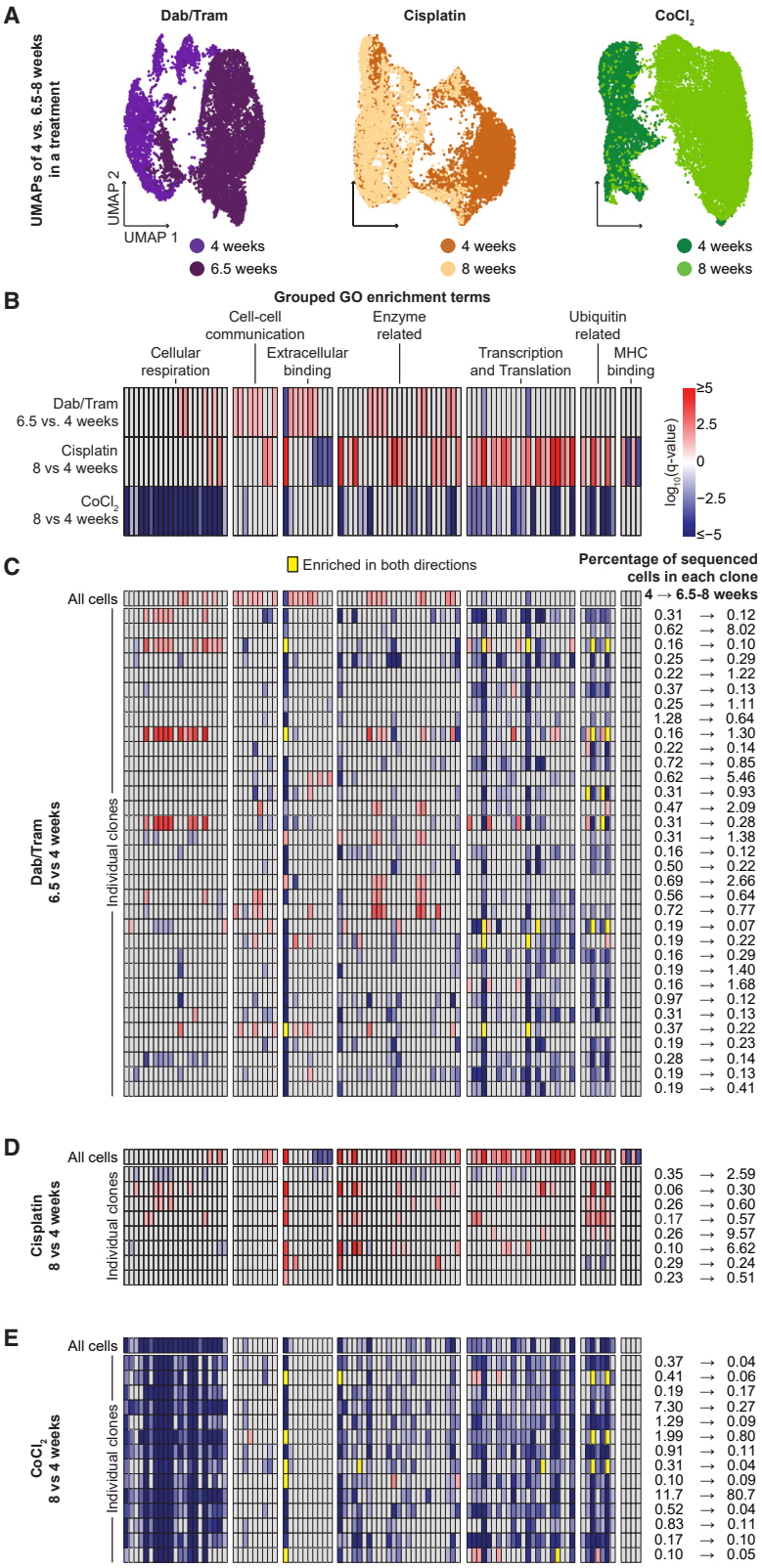

Figure 6. Prolonged treatment with the same agent causes population-level and clonal changes in pathway expression

(A) UMAPs (GEO: GSE253739) comparing cells sequenced after 4 and 6.5–8 weeks of treatment with (left) dabrafenib and trametinib (Dab/Tram), (middle) cisplatin, or (right) $CoCl_2$.

(B) We identified differentially expressed genes between 6.5–8 and 4 weeks of treatment with each agent. We then identified GO terms enriched after either the first round of treatment (blue) or the second round of treatment (red) based on the $\log_{10}$(q value) and $-\log_{10}$(q value) respectively and displayed these values in the heatmap. This is a measure of the confidence of enrichment, not an activity score. GO terms that were not significantly enriched, or failed other thresholds, in either direction for a condition are colored in gray. Enriched pathways were grouped into categories of related function, and the pathways that make up each group are detailed in Figure S7.

(C–E) Same analysis as performed in (B) with all of the cells from each condition (with that comparison displayed again) on a clone-by-clone basis for all clones with at least five cells in both rounds of treatment for Dab/Tram, cisplatin, and $CoCl_2$, respectively. On the right of each subpanel is displayed the percentage of total sequenced single cells per condition from each clone after each round of treatment. Pathways enriched in both directions are colored yellow.

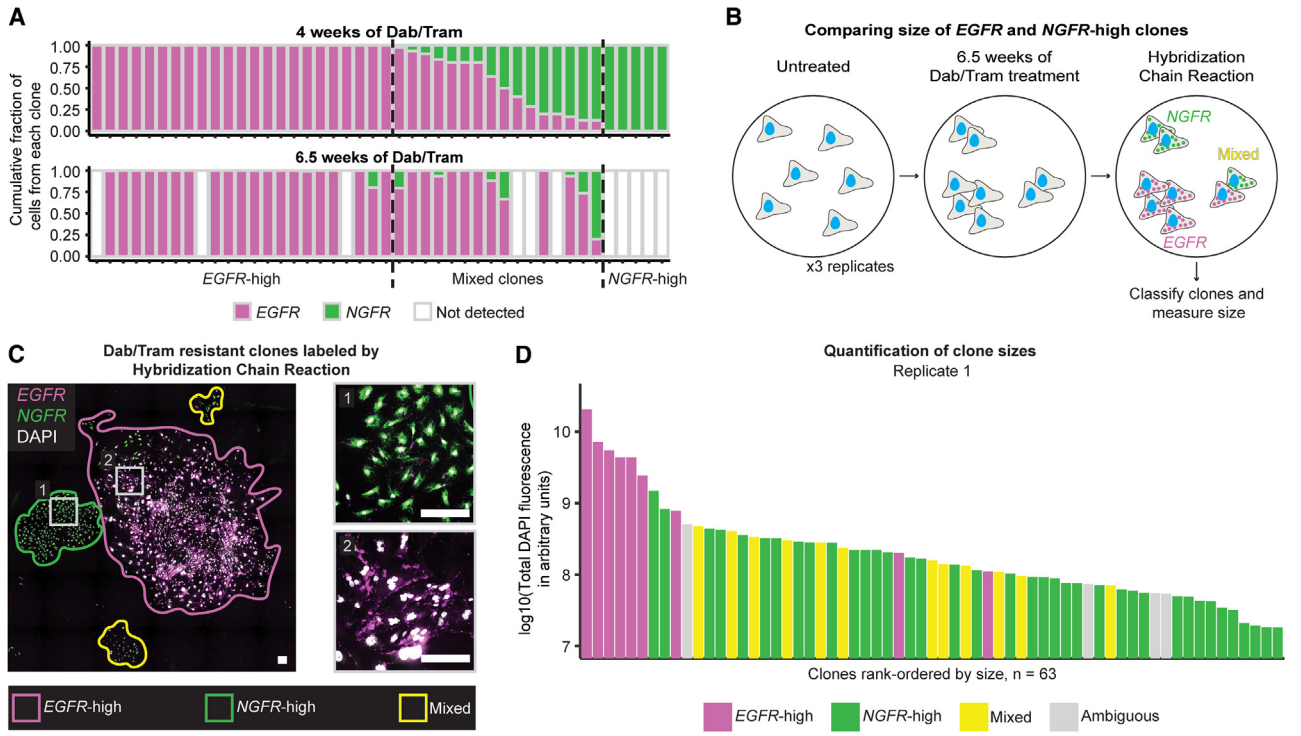

Figure 7. Clones with high *EGFR* expression exhibit enhanced survival when subjected to extended treatment with dabrafenib and trametinib

(A) Stacked colored bars represent the proportion of cells from each clone with at least five cells after initial treatment (4 weeks) with dabrafenib and trametinib (Dab/Tram) in the (magenta) *EGFR*-high cluster or (green) *NGFR*-high cluster (top). Dotted lines separate clones that are all *EGFR*-high, mixed *EGFR* and *NGFR* expression, and *NGFR*-high. Aligned below are the same clones after the second round of treatment (6.5 weeks) with Dab/Tram. Clones that still have greater than five cells are again colored by their proportion of cells in either the *EGFR*- or *NGFR*-high cluster, while clones that are no longer detected (less than five cells) are colored white.

(B) Experimental protocol for comparing the sizes of *EGFR*-high and *NGFR*-high clones.

(C) (Left) Example image (subset of replicate 2, from Figure S11B) showing dabrafenib- and trametinib-resistant cells labeling nuclei with DAPI (gray) and labeling *EGFR* (magenta spots) and *NGFR* (green spots) using hybridization chain reaction (HCR). Predominantly *EGFR*-high clones are circled in magenta, predominantly *NGFR*-high clones are circled in green, and mixed clones are circled in yellow. (Right) Cropped images highlighting that HCR labels individual transcripts with spots for *EGFR* and *NGFR*. Scale bars represent 200 μm.

(D) Quantification of replicate 1 clone sizes based on total DAPI fluorescence within circled clones from Figure S11A. Data are rank ordered based on clone size, and clones are colored based on their classification: *EGFR*-high, *NGFR*-high, mixed, or ambiguous. Quantification of replicates 2 and 3 are in Figures S11D and S11E.

more resistant to BRAFi compared with more differentiated melanocytic cells.[8,11] When looking at these same clones after treatment with dabrafenib and trametinib followed by $CoCl_2$, many of the *NGFR*-high clones also were lowly detected (Figures S10E and S10F). Conversely, the majority of these 44 clones that had any detection after treatment with dabrafenib and trametinib followed by cisplatin were originally *NGFR*-high or mixed, indicating that *NGFR* enrichment may indeed be beneficial for subsequent survival through cisplatin (Figure S10G). The enrichment and depletion of clones with specific expression patterns further supports the idea that gene expression states confer treatment-specific survival consequences.

To test whether these *NGFR*-high clones were dying or less captured in the scRNA-seq, we aimed to measure *EGFR* and *NGFR* across all resistant clones formed during prolonged treatment with dabrafenib and trametinib. For this purpose, we treated WM989 melanoma cells with dabrafenib and trametinib for 6.5 weeks and used hybridization chain reaction (HCR) to label *EGFR* and *NGFR* transcripts within resistant clones (Figure 7B). We classified clones based on the predominant cell type: *EGFR*-high (*EGFR*-high clones), *NGFR*-high (*NGFR*-high clones), or a mixture of both (mixed clones) (Figures 7C and S11A–S11C). After 6.5 weeks of treatment, we found that the largest clones were *EGFR*-high, while small *NGFR*-high clones were also present (Figures 7D, S11D, and S11E). This result suggests that the *NGFR*-high clones, which were undetected after 6.5 weeks in our clonal tracing experiment, were not dying off during the prolonged treatment; instead, they were growing at a slower rate than the *EGFR*-high clones. Consequently, the *EGFR*-high expression state is indicative of more growth during the prolonged treatment with dabrafenib and trametinib. More broadly, these data demonstrate that clonal differences in gene expression can predict clonal responses to prolonged treatment.

DISCUSSION

Tumor heterogeneity has been extensively studied for the role it plays in treatment resistance[1,2,5–11]; however, most of these

studies have focused on resistance to a single treatment.[2,4–8,10] Sequential treatment is a common approach for cancer treatment but has predominantly been studied through clinical trial data or at the bulk tumor/cell population level.[16,50–55] Here, we focus on the single-cell and single-clone level, addressing how resistant clones change in their abundance and transcriptional state over the course of sequential treatments. We combine imaging, scRNA-seq, and clonal tracking with cell barcoding to discover that individual resistant clones show highly variable responses to a second treatment, which highlights the importance of studying sequential treatment resistance at a clonal, rather than population level.

Our findings further support a growing body of evidence that resistance to treatment cannot be explained by single mechanisms acting in isolation.[10,56] Rather, resistance reflects a complex and dynamical process in which diverse and continuously evolving cellular states are generated.[9,27] Our work contributes another layer of phenotypic complexity by demonstrating that the diverse clones generated under treatment have differential sensitivities to subsequent treatments. We further connect the response of individual clones to specific gene expression states, thus supporting the notion that response to sequential treatments is nonrandom and occurs at the clonal level. The connection between phenotype and gene expression is similar to observations before treatment, where preexisting differences in the initial state of cells are predictive of treatment outcome.[8,26]

This study also contributes to our understanding of gene expression memory. While individual resistant clones have diverse transcriptional states, the cells within these clones are transcriptionally similar to each other. These states are heritable, such that the cells derived from a common parent cell have related transcriptional profiles. Such heritability has been measured in the absence of treatment and upon a single agent,[9,11,26,57] but here heritability of gene expression extends through prolonged and sequential treatments. We speculate that these clonal gene expression similarities are epigenetically encoded, but the full mechanisms remain to be elucidated. Furthermore, this heritability of gene expression is critical for our experimental design as it enables comparisons between the same clones receiving different treatments. Given that clones are still transcriptionally similar after the second treatment, this experimental and analytical framework could be easily scaled to include third and potentially even fourth rounds of treatment for assessing clonal dynamics on longer timescales and with additional treatments.

While our experimental design captures large resistant clones after treatment, it is less sensitive for smaller clones as our data are highly subsampled. The experimental framework relies on the ability of clones to proliferate for them to be captured at the different time points and evenly distributed across the samples. Thus, these data are not able to comment on non-proliferative states and/or very slow-cycling states, which have been implicated in pre-existing states associated with resistance.[4,5,58,59] While clones consisting of only one or a few cells can be detected in our data and others,[9] they are not likely to be present across multiple time points or treatment conditions (Figures S12A–S12G). Rather, because our experimental design emphasizes the most proliferative clones, we are best equipped to define how large clones respond and change during sequential treatment. Subsequent studies and alternative experimental designs would be needed to better capture the role of small clones in resistance.

In summary, we find that intraclonal similarities in gene expression are preserved over multiple months and across different treatments. Moreover, we show that interclonal differences in gene expression inform survival and proliferation through sequential and prolonged treatment, suggesting that the progression of resistance in these treatments is nonrandom. This knowledge lays the foundation for future work to target clonal states to prevent resistance to sequential and prolonged treatment.

STAR★METHODS

Detailed methods are provided in the online version of this paper and include the following:

- KEY RESOURCES TABLE
- RESOURCE AVAILABILITY
  - Lead contact
  - Materials availability
  - Data and code availability
- EXPERIMENTAL MODEL AND SUBJECT DETAILS
  - Cell lines and tissue culture
- METHOD DETAILS
  - Treatments
  - Treatment resistant clone experiments
  - Lentiviral packaging
  - Lentiviral transduction
  - Fluorescence-activated cell sorting (FACS) of barcoded cells
  - Single-cell RNA sequencing experiment
  - DNA barcode recovery from scRNA-seq
  - Creating DNA barcode ladders
  - DNA barcode recovery from gDNA
  - Validating that survival to treatment is deterministic with gDNA barcoding
  - Induced resistance experimental validation
  - EGFR and NGFR HCR RNA FISH
- QUANTIFICATION AND STATISTICAL ANALYSIS
  - Clone abundance heatmaps from gDNA
  - scRNA-seq analysis
  - Combining scRNA-seq and barcode data
  - Determining resistant clones for single-cell analysis
  - Analysis of transcriptional similarity based on treatment order
  - Clone similarity analysis
  - Induced resistance computational analysis
  - Gene ontology analysis
  - Pathway variability analysis
  - Computational analysis of induced resistance validation
  - Computational analysis of clone abundance during continued treatment of *EGFR*- and *NGFR*-high dabrafenib and trametinib resistant clones
  - Computational analysis of EGFR and NGFR HCR RNA FISH
- ADDITIONAL RESOURCES
  - Barcode Library

SUPPLEMENTAL INFORMATION

Supplemental information can be found online at https://doi.org/10.1016/j.cels.2024.01.011.

ACKNOWLEDGMENTS

We thank the members of the Shaffer Lab for input on the experiments and figures of the manuscript. We thank the Arjun Raj Lab at the University of Pennsylvania for the barcoding plasmid library and Nimbus Image software. A.J.F., P.E.W., and S.M.S. recognize support from Grants for Faculty Mentoring Undergraduate Research (A.J.F. and S.M.S., 2021; P.E.W. and S.M.S., 2022). S.M.S. recognizes support from the Wistar/Penn SPORE (P50 CA261608) and NIH Director's Early Independence Award (DP5OD028144).

AUTHOR CONTRIBUTIONS

Conceptualization, D.L.S., A.J.F., and S.M.S.; methodology, D.L.S., A.J.F., and S.M.S.; software, D.L.S., A.J.F., and R.J.V.V.; formal analysis, D.L.S., A.J.F., and R.J.V.V.; investigation, D.L.S., A.J.F., and P.E.W.; data curation, D.L.S., A.J.F., P.E.W., and R.J.V.V.; writing – original draft, D.L.S., A.J.F., P.E.W., R.J.V.V., and S.M.S.; writing – review & editing, D.L.S., A.J.F., P.E.W., R.J.V.V., and S.M.S.; visualization, D.L.S., A.J.F., P.E.W., R.J.V.V., and S.M.S.; funding acquisition, S.M.S., A.J.F., and P.E.W.; supervision, S.M.S.

DECLARATION OF INTERESTS

The authors declare no competing interests.

DECLARATION OF GENERATIVE AI AND AI-ASSISTED TECHNOLOGIES IN THE WRITING PROCESS

During the preparation of this work the author(s) used ChatGPT in order to help in paraphrasing and avoiding redundancy in our STAR Methods section. After using this tool/service, the author(s) reviewed and edited the content as needed and take(s) full responsibility for the content of the publication.

Received: March 31, 2023
Revised: November 14, 2023
Accepted: January 29, 2024
Published: February 23, 2024

REFERENCES

1. Nowell, P.C. (1976). The clonal evolution of tumor cell populations. Science *194*, 23–28.
2. Jin, J., Wu, X., Yin, J., Li, M., Shen, J., Li, J., Zhao, Y., Zhao, Q., Wu, J., Wen, Q., et al. (2019). Identification of Genetic Mutations in Cancer: Challenge and Opportunity in the New Era of Targeted Therapy. Front. Oncol. *9*, 263.
3. McGranahan, N., and Swanton, C. (2017). Clonal Heterogeneity and Tumor Evolution: Past, Present, and the Future. Cell *168*, 613–628.
4. Marine, J.-C., Dawson, S.-J., and Dawson, M.A. (2020). Non-genetic mechanisms of therapeutic resistance in cancer. Nat. Rev. Cancer *20*, 743–756.
5. Sharma, S.V., Lee, D.Y., Li, B., Quinlan, M.P., Takahashi, F., Maheswaran, S., McDermott, U., Azizian, N., Zou, L., Fischbach, M.A., et al. (2010). A chromatin-mediated reversible drug-tolerant state in cancer cell subpopulations. Cell *141*, 69–80.
6. Knoechel, B., Roderick, J.E., Williamson, K.E., Zhu, J., Lohr, J.G., Cotton, M.J., Gillespie, S.M., Fernandez, D., Ku, M., Wang, H., et al. (2014). An epigenetic mechanism of resistance to targeted therapy in T cell acute lymphoblastic leukemia. Nat. Genet. *46*, 364–370.
7. Spencer, S.L., Gaudet, S., Albeck, J.G., Burke, J.M., and Sorger, P.K. (2009). Non-genetic origins of cell-to-cell variability in TRAIL-induced apoptosis. Nature *459*, 428–432.
8. Shaffer, S.M., Dunagin, M.C., Torborg, S.R., Torre, E.A., Emert, B., Krepler, C., Beqiri, M., Sproesser, K., Brafford, P.A., Xiao, M., et al. (2017). Rare cell variability and drug-induced reprogramming as a mode of cancer drug resistance. Nature *546*, 431–435.
9. Goyal, Y., Busch, G.T., Pillai, M., Li, J., Boe, R.H., Grody, E.I., Chelvanambi, M., Dardani, I.P., Emert, B., Bodkin, N., et al. (2023). Diverse clonal fates emerge upon drug treatment of homogeneous cancer cells. Nature *620*, 651–659.
10. Vander Velde, R., Yoon, N., Marusyk, V., Durmaz, A., Dhawan, A., Miroshnychenko, D., Lozano-Peral, D., Desai, B., Balynska, O., Poleszhuk, J., et al. (2020). Resistance to targeted therapies as a multifactorial, gradual adaptation to inhibitor specific selective pressures. Nat. Commun. *11*, 2393.
11. Harmange, G., Hueros, R.A.R., Schaff, D.L., Emert, B., Saint-Antoine, M., Kim, L.C., Niu, Z., Nellore, S., Fane, M.E., Alicea, G.M., et al. (2023). Disrupting cellular memory to overcome drug resistance. Nat. Commun. *14*, 7130.
12. Beaumont, K.A., Hill, D.S., Daignault, S.M., Lui, G.Y.L., Sharp, D.M., Gabrielli, B., Weninger, W., and Haass, N.K. (2016). Cell Cycle Phase-Specific Drug Resistance as an Escape Mechanism of Melanoma Cells. J. Invest. Dermatol. *136*, 1479–1489.
13. Mishra, A., Wang, J., Shiozawa, Y., McGee, S., Kim, J., Jung, Y., Joseph, J., Berry, J.E., Havens, A., Pienta, K.J., et al. (2012). Hypoxia Stabilizes GAS6/Axl Signaling in Metastatic Prostate Cancer. Mol. Cancer Res. *10*, 703–712.
14. Widmer, D.S., Hoek, K.S., Cheng, P.F., Eichhoff, O.M., Biedermann, T., Raaijmakers, M.I.G., Hemmi, S., Dummer, R., and Levesque, M.P. (2013). Hypoxia contributes to melanoma heterogeneity by triggering HIF1α-dependent phenotype switching. J. Invest. Dermatol. *133*, 2436–2443.
15. Ravindran Menon, D., Das, S., Krepler, C., Vultur, A., Rinner, B., Schauer, S., Kashofer, K., Wagner, K., Zhang, G., Bonyadi Rad, E., et al. (2015). A stress-induced early innate response causes multidrug tolerance in melanoma. Oncogene *34*, 4448–4459.
16. Erdmann, S., Seidel, D., Jahnke, H.-G., Eichler, M., Simon, J.-C., and Robitzki, A.A. (2019). Induced cross-resistance of BRAFV600E melanoma cells to standard chemotherapeutic dacarbazine after chronic PLX4032 treatment. Sci. Rep. *9*, 30.
17. Stordal, B., Pavlakis, N., and Davey, R. (2007). Oxaliplatin for the treatment of cisplatin-resistant cancer: a systematic review. Cancer Treat. Rev. *33*, 347–357.
18. Fojo, A., Hamilton, T.C., Young, R.C., and Ozols, R.F. (1987). Multidrug resistance in ovarian cancer. Cancer *60*, 2075–2080.
19. Menzies, A.M., Long, G.V., and Murali, R. (2012). Dabrafenib and its potential for the treatment of metastatic melanoma. Drug Des. Dev. Ther. *6*, 391–405.
20. Lugowska, I., Koseła-Paterczyk, H., Kozak, K., and Rutkowski, P. (2015). Trametinib: a MEK inhibitor for management of metastatic melanoma. OncoTargets Ther. *8*, 2251–2259.
21. Piret, J.-P., Mottet, D., Raes, M., and Michiels, C. (2002). CoCl2, a chemical inducer of hypoxia-inducible factor-1, and hypoxia reduce apoptotic cell death in hepatoma cell line HepG2. Ann. N. Y. Acad. Sci. *973*, 443–447.
22. Wu, D., and Yotnda, P. (2011). Induction and testing of hypoxia in cell culture. J. Vis. Exp. https://doi.org/10.3791/2899.
23. Sherman, S.E., and Lippard, S.J. (1987). Structural aspects of platinum anticancer drug interactions with DNA. Chem. Rev. *87*, 1153–1181.
24. Biddy, B.A., Kong, W., Kamimoto, K., Guo, C., Waye, S.E., Sun, T., and Morris, S.A. (2018). Single-cell mapping of lineage and identity in direct reprogramming. Nature *564*, 219–224.
25. Weinreb, C., Rodriguez-Fraticelli, A., Camargo, F.D., and Klein, A.M. (2020). Lineage tracing on transcriptional landscapes links state to fate during differentiation. Science *367*, eaaw3381.

26. Emert, B.L., Cote, C.J., Torre, E.A., Dardani, I.P., Jiang, C.L., Jain, N., Shaffer, S.M., and Raj, A. (2021). Variability within rare cell states enables multiple paths toward drug resistance. Nat. Biotechnol. *39*, 865–876.

27. França, G.S., Baron, M., Pour, M., King, B.R., Rao, A., Misirlioglu, S., Barkley, D., Dolgalev, I., Ho-Tang, K., Avital, G., et al. (2022). Drug-induced adaptation along a resistance continuum in cancer cells. Preprint at bioRxiv. https://doi.org/10.1101/2022.06.21.496830.

28. Rose-John, S. (2020). Interleukin-6 signalling in health and disease. F1000Res *9*, 9.

29. Wang, Y., Niu, X.L., Qu, Y., Wu, J., Zhu, Y.Q., Sun, W.J., and Li, L.Z. (2010). Autocrine production of interleukin-6 confers cisplatin and paclitaxel resistance in ovarian cancer cells. Cancer Lett. *295*, 110–123.

30. Zhao, K., Lu, Y., Chen, Y., Cheng, J., and Zhang, W. (2020). Transcripts 202 and 205 of IL-6 confer resistance to Vemurafenib by reactivating the MAPK pathway in BRAF(V600E) mutant melanoma cells. Exp. Cell Res. *390*, 111942.

31. Masjedi, A., Hashemi, V., Hojjat-Farsangi, M., Ghalamfarsa, G., Azizi, G., Yousefi, M., and Jadidi-Niaragh, F. (2018). The significant role of interleukin-6 and its signaling pathway in the immunopathogenesis and treatment of breast cancer. Biomed. Pharmacother. *108*, 1415–1424.

32. Niu, N., Yao, J., Bast, R.C., Sood, A.K., and Liu, J. (2021). IL-6 promotes drug resistance through formation of polyploid giant cancer cells and stromal fibroblast reprogramming. Oncogenesis *10*, 65.

33. Wu, T., Hu, E., Xu, S., Chen, M., Guo, P., Dai, Z., Feng, T., Zhou, L., Tang, W., Zhan, L., et al. (2021). clusterProfiler 4.0: A universal enrichment tool for interpreting omics data. Innovation *2*, 100141.

34. Fedorenko, I.V., Abel, E.V., Koomen, J.M., Fang, B., Wood, E.R., Chen, Y.A., Fisher, K.J., Iyengar, S., Dahlman, K.B., Wargo, J.A., et al. (2016). Fibronectin induction abrogates the BRAF inhibitor response of BRAF V600E/PTEN-null melanoma cells. Oncogene *35*, 1225–1235.

35. Marusak, C., Thakur, V., Li, Y., Freitas, J.T., Zmina, P.M., Thakur, V.S., Chang, M., Gao, M., Tan, J., Xiao, M., et al. (2020). Targeting Extracellular Matrix Remodeling Restores BRAF Inhibitor Sensitivity in BRAFi-resistant Melanoma. Clin. Cancer Res. *26*, 6039–6050.

36. Straussman, R., Morikawa, T., Shee, K., Barzily-Rokni, M., Qian, Z.R., Du, J., Davis, A., Mongare, M.M., Gould, J., Frederick, D.T., et al. (2012). Tumour micro-environment elicits innate resistance to RAF inhibitors through HGF secretion. Nature *487*, 500–504.

37. Czarnecka, A.M., Bartnik, E., Fiedorowicz, M., and Rutkowski, P. (2020). Targeted Therapy in Melanoma and Mechanisms of Resistance. Int. J. Mol. Sci. *21*, 4576.

38. MacKay, C., Carroll, E., Ibrahim, A.F.M., Garg, A., Inman, G.J., Hay, R.T., and Alpi, A.F. (2014). E3 ubiquitin ligase HOIP attenuates apoptotic cell death induced by cisplatin. Cancer Res. *74*, 2246–2257.

39. Ko, T., and Li, S. (2019). Genome-wide screening identifies novel genes and biological processes implicated in cisplatin resistance. FASEB J. *33*, 7143–7154.

40. Ashton, T.M., McKenna, W.G., Kunz-Schughart, L.A., and Higgins, G.S. (2018). Oxidative Phosphorylation as an Emerging Target in Cancer Therapy. Clin. Cancer Res. *24*, 2482–2490.

41. Li, L.-D., Sun, H.-F., Liu, X.-X., Gao, S.-P., Jiang, H.-L., Hu, X., and Jin, W. (2015). Down-Regulation of NDUFB9 Promotes Breast Cancer Cell Proliferation, Metastasis by Mediating Mitochondrial Metabolism. PLoS One *10*, e0144441.

42. Andreatta, M., and Carmona, S.J. (2021). UCell: Robust and scalable single-cell gene signature scoring. Comput. Struct. Biotechnol. J. *19*, 3796–3798.

43. Nazarian, R., Shi, H., Wang, Q., Kong, X., Koya, R.C., Lee, H., Chen, Z., Lee, M.K., Attar, N., Sazegar, H., et al. (2010). Melanomas acquire resistance to B-RAF(V600E) inhibition by RTK or N-RAS upregulation. Nature *468*, 973–977.

44. Sun, C., Wang, L., Huang, S., Heynen, G.J.J.E., Prahallad, A., Robert, C., Haanen, J., Blank, C., Wesseling, J., Willems, S.M., et al. (2014). Reversible and adaptive resistance to BRAF(V600E) inhibition in melanoma. Nature *508*, 118–122.

45. Müller, J., Krijgsman, O., Tsoi, J., Robert, L., Hugo, W., Song, C., Kong, X., Possik, P.A., Cornelissen-Steijger, P.D.M., Geukes Foppen, M.H., et al. (2014). Low MITF/AXL ratio predicts early resistance to multiple targeted drugs in melanoma. Nat. Commun. *5*, 5712.

46. Ji, Z., Erin Chen, Y., Kumar, R., Taylor, M., Jenny Njauw, C.-N., Miao, B., Frederick, D.T., Wargo, J.A., Flaherty, K.T., Jönsson, G., et al. (2015). MITF Modulates Therapeutic Resistance through EGFR Signaling. J. Invest. Dermatol. *135*, 1863–1872.

47. Tsoi, J., Robert, L., Paraiso, K., Galvan, C., Sheu, K.M., Lay, J., Wong, D.J.L., Atefi, M., Shirazi, R., Wang, X., et al. (2018). Multi-stage Differentiation Defines Melanoma Subtypes with Differential Vulnerability to Drug-Induced Iron-Dependent Oxidative Stress. Cancer Cell *33*, 890–904.e5.

48. Tirosh, I., Izar, B., Prakadan, S.M., Wadsworth, M.H., 2nd, Treacy, D., Trombetta, J.J., Rotem, A., Rodman, C., Lian, C., Murphy, G., et al. (2016). Dissecting the multicellular ecosystem of metastatic melanoma by single-cell RNA-seq. Science *352*, 189–196.

49. Rambow, F., Rogiers, A., Marin-Bejar, O., Aibar, S., Femel, J., Dewaele, M., Karras, P., Brown, D., Chang, Y.H., Debiec-Rychter, M., et al. (2018). Toward Minimal Residual Disease-Directed Therapy in Melanoma. Cell *174*, 843–855.e19.

50. Sartor, O., and Gillessen, S. (2014). Treatment sequencing in metastatic castrate-resistant prostate cancer. Asian J. Androl. *16*, 426–431.

51. Modest, D.P., Pant, S., and Sartore-Bianchi, A. (2019). Treatment sequencing in metastatic colorectal cancer. Eur. J. Cancer *109*, 70–83.

52. Temraz, S., Mukherji, D., and Shamseddine, A. (2014). Sequencing of treatment in metastatic colorectal cancer: where to fit the target. World J. Gastroenterol. *20*, 1993–2004.

53. Johnson, D.B., Pectasides, E., Feld, E., Ye, F., Zhao, S., Johnpulle, R., Merritt, R., McDermott, D.F., Puzanov, I., Lawrence, D., et al. (2017). Sequencing Treatment in BRAF V600 Mutant Melanoma: Anti-PD-1 Before and After BRAF Inhibition. J. Immunother. *40*, 31–35.

54. Girotti, M.R., Gremel, G., Lee, R., Galvani, E., Rothwell, D., Viros, A., Mandal, A.K., Lim, K.H.J., Saturno, G., Furney, S.J., et al. (2016). Application of Sequencing, Liquid Biopsies, and Patient-Derived Xenografts for Personalized Medicine in Melanoma. Cancer Discov. *6*, 286–299.

55. Buck, S.A.J., Koolen, S.L.W., Mathijssen, R.H.J., de Wit, R., and van Soest, R.J. (2021). Cross-resistance and drug sequence in prostate cancer. Drug Resist. Updat. *56*, 100761.

56. Vander Velde, R., Shaffer, S., and Marusyk, A. (2022). Integrating mutational and nonmutational mechanisms of acquired therapy resistance within the Darwinian paradigm. Trends Cancer *8*, 456–466.

57. Shaffer, S.M., Emert, B.L., Reyes Hueros, R.A., Cote, C., Harmange, G., Schaff, D.L., Sizemore, A.E., Gupte, R., Torre, E., Singh, A., et al. (2020). Memory Sequencing Reveals Heritable Single-Cell Gene Expression Programs Associated with Distinct Cellular Behaviors. Cell *182*, 947–959.e17.

58. Roesch, A., Vultur, A., Bogeski, I., Wang, H., Zimmermann, K.M., Speicher, D., Körbel, C., Laschke, M.W., Gimotty, P.A., Philipp, S.E., et al. (2013). Overcoming intrinsic multidrug resistance in melanoma by blocking the mitochondrial respiratory chain of slow-cycling JARID1B(high) cells. Cancer Cell *23*, 811–825.

59. Roesch, A., Fukunaga-Kalabis, M., Schmidt, E.C., Zabierowski, S.E., Brafford, P.A., Vultur, A., Basu, D., Gimotty, P., Vogt, T., and Herlyn, M. (2010). A temporarily distinct subpopulation of slow-cycling melanoma cells is required for continuous tumor growth. Cell *141*, 583–594.

60. Subramanian, A., Tamayo, P., Mootha, V.K., Mukherjee, S., Ebert, B.L., Gillette, M.A., Paulovich, A., Pomeroy, S.L., Golub, T.R., Lander, E.S., et al. (2005). Gene set enrichment analysis: a knowledge-based approach for interpreting genome-wide expression profiles. Proc. Natl. Acad. Sci. USA *102*, 15545–15550.

61. Liberzon, A., Birger, C., Thorvaldsdóttir, H., Ghandi, M., Mesirov, J.P., and Tamayo, P. (2015). The Molecular Signatures Database (MSigDB) hallmark gene set collection. Cell Syst. *1*, 417–425.

62. Schneider, C.A., Rasband, W.S., and Eliceiri, K.W. (2012). NIH Image to ImageJ: 25 years of image analysis. Nat. Methods *9*, 671–675.

63. Korotkevich, G., Sukhov, V., Budin, N., Shpak, B., Artyomov, M.N., and Sergushichev, A. (2021). Fast gene set enrichment analysis. Preprint at bioRxiv. https://doi.org/10.1101/060012.

64. van der Walt, S., Schönberger, J.L., Nunez-Iglesias, J., Boulogne, F., Warner, J.D., Yager, N., Gouillart, E., and Yu, T.; scikit-image contributors (2014). scikit-image: image processing in Python. PeerJ *2*, e453.

65. Hao, Y., Hao, S., Andersen-Nissen, E., Mauck, W.M., 3rd, Zheng, S., Butler, A., Lee, M.J., Wilk, A.J., Darby, C., Zager, M., et al. (2021). Integrated analysis of multimodal single-cell data. Cell *184*, 3573–3587.e29.

66. Borcherding, N., Vishwakarma, A., Voigt, A.P., Bellizzi, A., Kaplan, J., Nepple, K., Salem, A.K., Jenkins, R.W., Zakharia, Y., and Zhang, W. (2021). Mapping the immune environment in clear cell renal carcinoma by single-cell genomics. Commun. Biol. *4*, 122.

67. Acheampong, K.K., Schaff, D.L., Emert, B.L., Lake, J., Reffsin, S., Shea, E.K., Comar, C.E., Litzky, L.A., Khurram, N.A., Linn, R.L., et al. (2021). Subcellular Detection of SARS-CoV-2 RNA in Human Tissue Reveals Distinct Localization in Alveolar Type 2 Pneumocytes and Alveolar Macrophages. mBio *13*, e0375121.

STAR★METHODS

KEY RESOURCES TABLE

REAGENT or RESOURCE	SOURCE	IDENTIFIER
Antibodies		
Anti-CD130 Mouse Monoclonal Antibody (PE (Phycoerythrin)) [clone: 2E1B02]	BioLegend	Cat#10760-758; RRID: AB_2563402
Chemicals, peptides, and recombinant proteins		
Dabrafenib	Cayman Chemical	16989-10; CAS: 1195765-45-7
Trametinib (#1)	Cayman Chemical	16292-50; CAS: 871700-17-3
Trametinib (#2)	SelleckChem	Cat#S2673; CAS: 871700-17-3
Cobalt Chloride, hexahydrate, crystal	Spectrum Chemical Manufacturing Corporation	Cat#18609836; CAS: 7791-13-1
Doxorubicin hydrochloride	Tocris Bioscience	CAS: 25316-40-9
MES, 1.0M buffer solution, pH 5.0	Thermo Scientific	Cat#AAJ61960AK; CAS:145224-94-8
Polyethylenimine, Linear, MW 25000	Polysciences	Cat#23966-1; CAS: 9002-98-6, 26913-06-4
Polybrene	MilliporeSigma	TR1003G; Cat#638132
SSC (20X), RNase-free	Invitrogen	Cat#AM9765
Formamide (Deionized)	Invitrogen	Cat#AM9344
Dextran Sulfate Sodium Salt	Fisher Scientific	Cat#BP1585-100; CAS: 9011-18-1
Citric Acid Anhydrous (Crystalline)	Fisher Scientific	Cat#BP339-500; CAS: 77-92-9
Heparin sodium salt from porcine intestinal mucosa	Sigma Aldrich	H5515-25KU; CAS: 9041-08-1
Denhardt's Solution (50X)	Invitrogen	Cat#750018
Tween 20, 100% Nonionic Detergent	Bio-Rad	Cat#1705017
Critical commercial assays		
Qubit dsDNA Quantification Assay Kits	Invitrogen	Cat#Q32854;
Bioanalyzer High Sensitivity DNA Kit	Agilent	Cat#5067-4626
NextSeq 500/550 High Output Kit v2.5 (75 Cycles)	Illumina	Cat#20024906
NextSeq 500/550 High Output Kit v2.5 (150 Cycles)	Illumina	Cat#20024904
NEBNext Q5 HotStart HiFi PCR Master Mix	New England Biolabs	Cat#M0543S
AMPure XP magnetic beads	Beckman Coulter	Cat#A63881
QIAmp DNA Mini Kit	Qiagen	Cat#51304
10X Genomics 3' v3.1 Dual index Single-Cell gene expression kit	10X Genomics	Cat#PN-1000269
Deposited data		
Raw and processed scRNA-seq data	This paper	GEO: GSE253739
scRNA-seq data of untreated WM989 cells	Harmange et al.[11]	GEO: GSE237228
Raw and processed barcoding sequencing data	This paper	Figshare: https://figshare.com/projects/Clonal_differences_underlie_variable_responses_to_sequential_and_prolonged_treatment/192653; Figshare: https://doi.org/10.6084/m9.figshare.25029338; Figshare: https://doi.org/10.6084/m9.figshare.25024466; Figshare: https://doi.org/10.6084/m9.figshare.25024463; Figshare: https://doi.org/10.6084/m9.figshare.25021745; Figshare: https://doi.org/10.6084/m9.figshare.25021730

(*Continued on next page*)

Continued

REAGENT or RESOURCE	SOURCE	IDENTIFIER
Fully normalized scRNA-seq Seurat object	This paper	Figshare: https://figshare.com/projects/Clonal_differences_underlie_variable_responses_to_sequential_and_prolonged_treatment/192653; Figshare: https://doi.org/10.6084/m9.figshare.25021742
Molecular Signals Database Hallmark Gene Sets (v2022.1)	Subramanian et al.[60]; Liberzon et al.[61]	https://www.gsea-msigdb.org/gsea/msigdb/
Experimental models: Cell lines		
WM989	Gift from Meenhard Herlyn Lab	RRID:CVCL_0B84
HEK293T	Gift from Ivan Maillard Lab	RRID:CVCL_0063
Oligonucleotides		
Primers for amplifying barcodes from gDNA and cDNA, see Table S1	This paper; Harmange et al.[11]; Goyal et al.[9]	N/A
Recombinant DNA		
LentiEFS_GFP_100bp_barcode_v1	Raj Lab: Emert et al.[26]	https://www.protocols.io/view/barcode-plasmid-library-cloning-5qpvon6yxl4o/v1; https://benchling.com/shaffer_lab/f/lib_6JXLhfQH-plasmids/seq_BUIxqCk0-lentiefs_gfp_100bp_barcode_v1/edit?m=slm-GJ609ijArVWmkT8mk8zr
psPAX2 plasmid	psPAX2 was a gift from Didier Trono	Addgene plasmid #12260
pMD2.G plasmid	pMD2.G was a gift from Didier Trono	Addgene plasmid #12259
Software and algorithms		
ImageJ	Schneider et al.[62]	https://imagej.nih.gov/ij/
fgsea (v1.22.0)	Korotkevich et al.[63]	https://bioconductor.org/packages/release/bioc/html/fgsea.html
Scikit-image (v0.21.0)	van der Walt et al.[64]	https://scikit-image.org/
Nimbus	Arjun Raj Lab	https://github.com/Kitware/UPennContrast; https://github.com/arjunrajlaboratory/ImageAnalysisProject/
Barcode Analysis	Harmange et al.[11]	https://github.com/SydShafferLab/BarcodeAnalysis
Seurat (v4)	Hao et al.[65]	https://satijalab.org/seurat/articles/get_started.html
CellRanger (5.0.1)	10X Genomics	https://www.10xgenomics.com/support/software/cell-ranger/latest/release-notes/cr-release-notes
UCell (v2.4.0)	Andreatta and Carmona[42]	https://www.bioconductor.org/packages/release/bioc/html/UCell.html
clusterProfiler (v4.8.3)	Wu et al.[33]	https://bioconductor.org/packages/release/bioc/html/clusterProfiler.html
Escape (v1.8.0)	Borcherding et al.[66]	https://bioconductor.org/packages/release/bioc/html/clusterProfiler.html
Custom analysis scripts for this paper	This paper	https://github.com/SydShafferLab/Schaff_and_Fasse_Cell_Systems; Zenodo: https://doi.org/10.5281/zenodo.10552083

RESOURCE AVAILABILITY

Lead contact

Further information and requests for resources and reagents should be directed to and will be fulfilled by the lead contact, Sydney Shaffer (sydshaffer@gmail.com).

Materials availability

This study did not generate new materials.

Data and code availability

Raw and processed scRNA-seq data have been deposited at SRA and GEO (GEO: GSE253739) and are publicly available as of the date of publication. Raw and processed barcode sequencing data has been deposited at figshare (Figshare: https://figshare.com/projects/Clonal_differences_underlie_variable_responses_to_sequential_and_prolonged_treatment/192653, Figshare: https://doi.org/10.6084/m9.figshare.25029338, Figshare: https://doi.org/10.6084/m9.figshare.25024466, Figshare: https://doi.org/10.6084/m9.figshare.25024463, Figshare: https://doi.org/10.6084/m9.figshare.25021745, Figshare: https://doi.org/10.6084/m9.figshare.25021730). The merged and normalized seurat object including RNA and clonal barcode reads has been deposited at figshare (Figshare: https://figshare.com/projects/Clonal_differences_underlie_variable_responses_to_sequential_and_prolonged_treatment/192653, Figshare: https://doi.org/10.6084/m9.figshare.25021742). All other data reported in this paper will be shared by the lead contact upon request. Accession numbers are listed in the key resources table.

All original code has been deposited at GitHub using Zenodo (https://github.com/SydShafferLab/Schaff_and_Fasse_Cell_Systems, DOI: Zenodo: https://doi.org/10.5281/zenodo.10552083) and is publicly available as of the date of publication. DOIs are listed in the key resources table.

Any additional information required to reanalyze the data reported in this paper is available from the lead contact upon request.

EXPERIMENTAL MODEL AND SUBJECT DETAILS

Cell lines and tissue culture

We performed all experiments on WM989 A6-G3 melanoma cell lines, including variations with a GFP nuclear reporter (H2B-GFP). WM989 A6-G3 cells were derived from WM989 cells and single-cell bottlenecked twice. WM989 A6-G3 cell lines were authenticated and validated as mycoplasma negative.[11] We cultured all WM989-derived lines in TU2% media consisting of 78% MCDB 153, 20% Leibovitz's L-15, 2% FBS, 1.68 mM $CaCl_2$, 50 U/mL penicillin, and 50 ug/mL streptomycin. We passaged non-treated cells with 0.05% trypsin-EDTA, and treatment-resistant cells were passaged with 0.25% trypsin-EDTA. For lentivirus packaging, HEK293T cells were cultured in DMEM containing 10% FBS, 50 U/mL penicillin, and 50 ug/mL streptomycin. We passaged HEK293Ts with 0.05% trypsin-EDTA. All cells were maintained at 37°C and 5% CO_2.

For experiments using fixed cells, we washed cells with 1x PBS (Invitrogen, AM9625), added 4% formaldehyde in 1x PBS (Fisher, BPBP531500) for 10 minutes, performed two more washes with 1x PBS, and stored at 4°C in 70% ethanol until cells were stained.

METHOD DETAILS

Treatments

We made stock solutions of 500 μM dabrafenib (Cayman, 16989-10), 5 μM trametinib (Cayman, 16292-50 and SelleckChem, 871700-17-3), 50 μM doxorubicin (Tocris Bioscience, 25316-40-9), and 25 mM $CoCl_2$ (Spectrum Chemical Manufacturing Corporation, 18609836) as follows: dabrafenib, trametinib, and doxorubicin in DMSO, cisplatin in 154 mM NaCl, and CoCl2 in nuclease-free water. For the single-cell experiments, we diluted all agents in culture medium to a final concentration of 15 μM cisplatin, 50 nM Doxorubicin, 200 μM $CoCl_2$, and 2.5 nM trametinib plus 250 nM dabrafenib for combined dabrafenib/trametinib treatment unless stated otherwise. MES buffer at 1 M, pH 5.0 (Thermo Scientific, AAJ61960AK) was used to make acidic TU2% media at 6.25 pH.

Treatment resistant clone experiments

We treated H2B-GFP WM989 cells with one of each of the following treatments for four weeks. For cells treated with 200 μM $CoCl_2$ in TU2% medium, we performed a media change every three to four days, each time treating with $CoCl_2$ treated media. For cells treated with 15 μM cisplatin, we treated with cisplatin treated TU2% medium for the first three days, then every following media change used normal TU2%. For cells treated with 250 nM dabrafenib and 2.5 μM trametinib, we performed a media change every three to four days, each time treating with dabrafenib and trametinib treated TU2% medium. For the next four weeks of treatment, we treated cells with a second round of treatment with cisplatin, $CoCl_2$ or a combination of dabrafenib and trametinib using the corresponding protocol for weeks five through eight. We imaged cells at four weeks (following the first round of treatment) and eight weeks (following the second round treatment) in the GFP channel (20 msec exposure). Images were contrasted using custom python scripts.

Lentiviral packaging

We packaged barcodes into lentivirus following the procedure outlined for the Rewind library.[26] In brief, HEK293T cells were cultured in three 10 cm plates until nearing confluency. For all three plates plus one half a plate worth of excess solution, we combined 1750 μL Opti-MEM (Gibco, 31985062) with 280 μL PEI (Polysciences, 23966-1) in one tube while another 1750 μL Opti-MEM was mixed with 35 μg (29.2 μL) barcode plasmid, 26.25 μg (20.9 μL) psPAX2 (Addgene #12260), and 17.5 μg (30.2 μL) VSVG (pMD2.G, Addgene #12259) in a second tube. We incubated each tube at room temperature for five minutes before combining them, vortexing, and incubating for an additional 15 minutes. We then slowly added 1106 μl of the mixed solution to each of the three 10 cm plates. After six hours, we discarded the media and replaced it with seven ml of DMEM. After 24 hours and confirming GFP expression, we collected

the virus-containing media into a conical tube stored at 4°C and replaced it with another seven mL of fresh media. After collecting virus twice more at 24 hour intervals, we centrifuged the virus-containing media at 3000 rpm for five minutes. We collected the supernatant and passed it through a 0.45 μm filter (Millipore Sigma, SE1M003M00). Finally, we made 1 mL aliquots and placed them at -80°C for storage.

Lentiviral transduction

For experiments involving the transduction of WM989 A6-G3 with barcode virus, we seeded cells in six-well plates at 300,000 cells per well and dropwise added 32 μL (as determined by titration for 20-25% infection efficiency) of freshly thawed virus. We then centrifuged the cells at 1750 RPM for 25 minutes and incubated overnight at 37°C. The following morning, we removed the media, washed the cells once with DPBS, and added fresh TU2% media.

Fluorescence-activated cell sorting (FACS) of barcoded cells

Three days after transducing cells with the GFP-barcode virus, we performed fluorescence-activated cell sorting to isolate GFP-expressing, barcoded WM989 A6-G3 cells. We used 0.05% trypsin-EDTA to obtain single-cell suspensions, neutralized with TU2%, washed the cell pellet with 1% BSA-DPBS, and resuspended in 1% BSA-DPBS containing DAPI. We passed the resuspended cells through a FACS cell strainer (Falcon, 352235) prior to FACS. We performed sorting on a Beckman Coulter MoFlo Astrios sorter with a 100 μm nozzle. We gated for singlets and live cells, then sorted for GFP-positive cells.

Single-cell RNA sequencing experiment

For the single-cell experiment outlined in Figure 2A, we trypsinized cells that had been sorted for being GFP-barcode positive the previous day and replated 425,000 starting cells. We allowed these cells to double roughly 5.5 times so that we had ~45 cells per clone. We pelleted and froze $^1/_3$ of these cells at -80°C for later barcode sequencing from gDNA. We then plate 225,000 cells in 18 x 10 cm plates each (54 total) for treatment with either a combination of dabrafenib and trametinib, $CoCl_2$, or cisplatin. The following day, we began treating the cells. For combination treatment with dabrafenib and trametinib and for treatment with $CoCl_2$, treated media was added every three to four days for four weeks. For cisplatin treatment, we treated cells for three days before replacing with normal media which was maintained until the end of four weeks. After four weeks, resistant cells were trypsinized. From each treated population, we removed ¼ of the surviving cells for scRNA-seq of ~7,000 cells and barcode sequencing from gDNA of the remaining cells. The remaining cells from each population were split evenly to receive the three secondary treatments for an additional four weeks, as previously described. After the second round of treatment was complete, we performed scRNA-seq on ~10,000 cells and froze the remaining at -80°C for barcode sequencing from gDNA. One sample, combination treatment of dabrafenib and trametinib into dabrafenib and trametinib, was collected after only 2.5 weeks of secondary treatment as the cells were nearing confluency.

We performed all scRNA-seq using the 10X Genomics 3' v3.1 Dual index Single-Cell gene expression kit (10X Genomics, PN-1000269) on a 10X Chromium Controller. We quantified libraries using the Qubit dsDNA High Sensitivity Assay (Invitrogen, Q32854) and the Agilent Bioanalyzer High Sensitivity DNA Kit (Agilent, 5067-4626). We then diluted libraries to four nM and pooled samples. We sequenced pooled samples on a NextSeq 500 with 75 cycle high output kits (Illumina, 20024906) using 28 cycles for read one, 10 cycles for each index, and 43 cycles for read two.

DNA barcode recovery from scRNA-seq

We amplified DNA barcodes from excess full-length cDNA generated during the 10X workflow as described previously.[11] In brief, we performed targeted amplification of the barcode from the full-length cDNA using primers with Illumina adapter sequences, sample indices, and staggered bases of different lengths from Goyal et al.[9] and Harmange et al.[11] (Table S1). For each sample, we diluted cDNA to 8.75 ng/μL and performed PCR reactions using 5 μL cDNA, 500 nM primers, 25 μL NEBNext Q5 HotStart HiFi PCR Master Mix (NEB, M0543S), and nuclease-free water for a total volume of 50 μL. We ran reactions on a thermal cycler using the following settings: 98°C for 30 seconds, 13 cycles of 98°C for 10 seconds and 65°C for two minutes, followed by a final step at 65°C for five minutes. After PCR, we purified the libraries using 0.7x (35 μL) AMPure XP magnetic beads (Beckman Coulter, A63881) followed by two 80% ethanol washes and a final elution of our purified barcodes in 20 μL of nuclease-free water per sample. We quantified purified libraries using Qubit dsDNA High Sensitivity Assay (Invitrogen, Q32854) and the Agilent Bioanalyzer High Sensitivity DNA Kit (Agilent, 5067-4626). We diluted libraries and sequenced an equimolar pool of all samples on a NextSeq 500 using a 150 cycle mid output kit (Illumina, 20024904) using 28 cycles for read one to capture the 10X barcodes and UMIs, eight cycles for each index, and 123 cycles on read two to capture the clone DNA barcodes.

Creating DNA barcode ladders

To create standardized ladders to relate gDNA barcode reads to number of cells, we used FACS as described above to sort barcoded, GFP-positive single cells into each well of four 96-well plates and cultured the cells in untreated TU2% media as described above. These single cells were allowed to expand into single-clone colonies which we grew to confluence in 10 cm plates, at which point we harvested a portion of each clone for barcode sequencing. We left the remainder to expand further. We performed barcode library preparations on the harvested cells from each clone as described below by isolating gDNA, PCR amplifying the barcode sequence, and performing double-sided bead cleanup. These sequences were then sent for Sanger sequencing (Eurofins

Genomics). From the ten clones sequenced, we selected six to use as ladder clones which contained correct conserved regions and had no ambiguous bases. We selected two clones each to be high, medium, and low abundance clones in the ladder, corresponding to 1000, 500, or 50 cells. We then trypsinized and counted live cells from each clone via hemocytometer and added the correct number of cells from each clone into tubes which were stored at -80°C.

DNA barcode recovery from gDNA

We performed barcode library preparations from genomic DNA (gDNA) as previously described with slight modifications.[26] In brief, we thawed cell pellets that had been stored at -80°C and added a "ladder" of cells with known barcode sequences and known initial cell numbers (two replicates each of 50, 500, and 1000 cells per clone) to each pellet (Figure S2A). We then isolated gDNA from cells using the QIAmp DNA Mini Kit (QIAGEN, 51304), following the spin protocol for DNA purification from blood or bodily fluids. We then amplified DNA barcodes from gDNA using primers with Illumina adapter sequences, sample indices, and staggered bases of different lengths from Harmange et al.[11] (Table S1). For each sample, we performed several PCR reactions (utilizing 20-40% of the total isolated gDNA), each containing 500 ng of gDNA, 500 nM primers, 25 μL of the NEBNext Q5 HotStart HiFi PCR Master Mix (NEB, M0543S), and nuclease-free water to a final volume of 50 μL. We ran reactions on a thermal cycler using the following settings: 98°C for 30 seconds, 23 cycles of 98°C for 10 seconds and 65°C for 40 seconds, and 65°C for five minutes. After PCR, we pooled individual reactions from the same sample before cleaning. We performed double-sided library purifications on the pooled samples using first 0.6x (30 μL x the number of pooled reactions) AMPure XP magnetic beads (Beckman Coulter, A63881) and keeping the supernatant. To the supernatant, we added 1.2x (30 μL x the number of pooled reactions) AMPure XP magnetic beads and washed twice with 80% ethanol. We eluted our purified barcodes from the beads using nuclease-free water (20 μL x the number of pooled reactions). We quantified purified libraries using Qubit dsDNA High Sensitivity Assay (Invitrogen, Q32854) and the Agilent Bioanalyzer High Sensitivity DNA Kit (Agilent, 5067-4626). We diluted and made an equimolar pool of all libraries for sequencing on a NextSeq 500 using a 150 cycle mid output kit (Illumina, 20024904) using 151 cycles for read one to capture the clone DNA barcodes and eight cycles for each index.

Validating that survival to treatment is deterministic with gDNA barcoding

We transduced WM989 A6-G3 melanoma cells with our barcode library (see STAR Methods section "lentiviral transduction") with the only variation being we added 8 μg/ml polybrene (MilliporeSigma, TR1003G) along with the virus and sorted out 350,000 barcoded cells. We then allowed the population to double ~6 times. We randomly split the cells into 12 samples for six different treatments with two samples receiving each treatment. The treatments were as follows: dabrafenib (1 μM), trametinib (10 nM), $CoCl_2$ (200 μM), cisplatin (5 μM), doxorubicin (50 nM), and 6.25 pH acidic media. For each sample, cells were plated at 320,000 cells per 10cm plate. The following day, we began treating the cells every three to four days. In this experiment, cisplatin received two weeks of treatment followed by two weeks of normal media and doxorubicin treated cells received 2.5 weeks of treatment followed by 1.5 weeks of normal media while dabrafenib, trametinib, $CoCl_2$, and acid treated cells received treatment for four weeks. After four weeks, the surviving cells were collected and frozen at -80°C until DNA barcode recovery was performed (see STAR Methods section "DNA barcode recovery from gDNA"). For the 12 samples, we performed two separate PCR reactions with 250 ng of input gDNA with 25 amplification cycles, did a double-sided library purification, and sequenced an equimolar pool of the libraries (see STAR Methods section "DNA barcode recovery from gDNA"). These samples did not include a cell barcode ladder.

Using custom R scripts, we combined the reads from the two sequencing samples that corresponded to each of the original 12 biological samples. We then normalized the reads by sequencing depth to obtain the reads per million (RPM) for each barcode in each of the 12 samples. Finally, we generated scatterplots of the detection of each barcode between the two biological replicates for each of the treatments and calculated the Pearson correlation coefficient (Figures S2B–S2E).

Induced resistance experimental validation

To test whether a specific cellular state (IL6ST-high) is a marker of induced resistance to a second treatment, we performed an experiment in which we first generated resistance to one treatment, sorted out cells based on marker expression, and then applied the second treatment. For this experimental design, we first treated WM989 A6-G3 melanoma cells with a combination of dabrafenib (125nM) and trametinib (1.25nM) for four weeks. Here, we used half of the dosage used in the clonal tracing experiment to increase our resistant cell numbers for sorting and replating. We then sorted the surviving resistant cells based on their expression of CD130 (IL6ST), which was identified in the scRNA-seq as a marker of cells predicted to be resistant to $CoCl_2$ following dabrafenib and trametinib treatment. We pooled resistant cells using 0.25% Trypsin-EDTA and stained them with 50 μg/mL PE anti-human CD130 antibody at a 1:200 dilution (Biolegend, 10760-758). Using the Beckman Coulter MoFlo Astrios sorter, we sorted cells as 'IL6ST-high' if they were in the top 30% of IL6ST expression and categorized cells as 'IL6ST-low' if they were in the bottom 30% of IL6ST expression. Following sorting, we replated the cells at three different densities in 6-well plates with 500, 1000, or 5000 cells per well. We then treated them for four weeks with $CoCl_2$ (25mM). We performed two biological replicates for this experiment. With the second biological replicate (Figures 5F and S6E), we added an additional plate to account for potential errors in counting. For this plate, we seeded 5000 cells per well into a 6-well plate and fixed the plate immediately after seeding for counting. After four weeks, we formaldehyde-fixed the treated cells, stained them with DAPI, and imaged them on a Nikon Eclipse Ti2 microscope. For each well, we acquired a 12x12 scan at 4X magnification with 500 msec exposure using a filter set for DAPI.

EGFR and NGFR HCR RNA FISH

We seeded 20,000 WM989 A6-G3 cells per well into three wells of a glass-bottom 6-well plate (CellVis, P6-1.5H-N), and treated with dabrafenib and trametinib. After 6.5 weeks of treatment, we fixed the cells using formaldehyde (as described in the Cell lines and tissue culture section). We performed HCR RNA FISH on the treated and fixed cells as described by Acheampong et al.[67] with minor modifications. We pre-hybridized samples with 0.6 mL of hybridization buffer (5x SSC (Invitrogen, AM9765), 30% formamide (Ambion, AM9344), 10% dextran sulfate (Fisher Scientific, BP1585–100), 9 mM citric acid (pH 6.0) (Fisher Scientific, BP339–500), 50 μg/mL of heparin (Sigma-Aldrich, H5515-25KU), 1x Denhardt solution (Invitrogen, 750018), and 0.1% Tween 20 (Bio-Rad, 1705017)) for 30 minutes at 37°C. We then replaced the pre-hybridization buffer with 0.6 mL of hybridization buffer containing 2.4 pmol each of EGFR and NGFR HCR RNA FISH. We covered the samples with a glass coverslip, humidified the samples by filling empty wells with 2x SSC, and incubated at 37°C for seven hours. We then washed samples four times for five minutes each at 37°C with wash buffer (5x SSC, 30% formamide, 9 mM citric acid (pH 6.0), 50 μg/mL heparin, and 0.1% Tween 20) followed by two washes with 5x SSCT (5x SSC with 0.1% Tween 20) at room temperature. We next added 0.6 mL of amplification buffer (5x SSC, 10% dextran sulfate, and 0.1% Tween 20) and let them incubate at room temperature for 30 minutes. While the samples incubated in pre-amplification buffer, we brought 1.2 uL per well of 3 μM of Molecular Instruments HCR hairpins conjugated to Alexa Fluor 488 (EGFR) and Alexa Fluor 647 (NGFR) in individual PCR tubes to 95°C and allowed them to cool at a rate of 0.08°C/s to room temperature. We then pooled these hairpins in 0.6 mL per well of amplification buffer and added them to the sample along with a glass coverslip. The samples in the amplification buffer were incubated at room temperature for 16 h overnight away from light. Finally, we washed the samples five times for five minutes each with 5x SSCT and stained with DAPI in 2x SSC.

For imaging, we used a Nikon Eclipse Ti2 microscope and acquired 20x20 scans at 10X magnification using filters for DAPI, GFP, and Atto647. We used exposure times of 100 msec for DAPI, 400 msec for Alexa Fluor 488 (EGFR), and 1 s for Alexa Fluor 647 (NGFR).

QUANTIFICATION AND STATISTICAL ANALYSIS

Clone abundance heatmaps from gDNA

We calculated the ln(Reads Per Million (RPM) + 1) of clones with at least two reads in the pre-treatment sample or with reads greater than one of the two corresponding 50-cell ladder clones in a given initial treatment sample or any subsequent treatment samples. We then subsampled and rank-ordered 100 clones for display in the heatmaps in Figures 2C and S2F and displayed the number of clones with at least one sequencing read.

scRNA-seq analysis

We generated gene count matrices using the CellRanger software 5.0.1 (10X Genomics) with the 2020-A hg38 reference genome, and we performed downstream analyses in the Seurat v4 package.[65] We also used CellRanger Feature Barcode technology to merge our custom clone barcodes sequencing with scRNA-seq data. For each sample, we filtered to remove cells with high RNA count indicating doublets, low numbers of genes detected, and a high percentage of mitochondrial reads. Data was processed using NormalizeData, FindVariableFeatures, ScaleData, RunPCA, FindNeighbors, FindClusters, and RunUMAP in that order. Downstream analyses are described in their associated methods sections.

For calculations of the percentage of cells in a condition expressing a gene, a cutoff of greater than one count was used.

Combining scRNA-seq and barcode data

To identify clone barcodes present in our sequencing data, we used a custom pipeline described by Harmange et al.[11] and available here: https://github.com/SydShafferLab/BarcodeAnalysis. Briefly, this pipeline takes in FASTQ files containing sequencing reads of barcodes from both gDNA and cDNA and identifies unique barcode sequences throughout all files. This code then collapses highly similar sequences with a Levenshtein distance of eight or less that are likely the same barcode which contains small alterations caused by small point mutations, PCR artifacts, or sequencing artifacts. The pipeline outputs a reference file along with both gDNA and cDNA FASTQ files that were corrected for collapsed barcodes. The corrected cDNA FASTQ files and the reference file can be input into the CellRanger Feature Barcode pipeline to generate count matrices and link cDNA barcode sequencing reads with their cell of origin based on the 10X barcode and UMI. Additionally, this pipeline separately outputs a list of total counts per barcode from either the cDNA and gDNA samples sequenced from each condition.

After combining scRNA-seq with cDNA barcode sequencing data, we found that some cells had reads from multiple barcodes. To assign the dominant barcode to each cell, we separately set a reads-based cutoff for each sequencing sample that maximized the total number of cells that only had a single barcode above the cutoff number of reads. In the case that a cell contained multiple barcodes each with reads above the cutoff, we assigned that cell a dominant barcode only if the reads of the highest detected barcode were 3-fold higher than the second highest detected barcode. Cells without a dominant barcode were excluded from clone-based analyses.

Determining resistant clones for single-cell analysis

From the gDNA reads, we identified resistant clones in each sample as any clone with more reads than the lower number of reads associated with one of the two 50-cell ladder clones in that sample. We supplemented these lists by adding clones

which had at least one read in the sample as well as more than 50 cells-equivalency gDNA reads within any sample from the same sequential treatment group (e.g. in either cisplatin, cisplatin to cisplatin, cisplatin to $CoCl_2$, or cisplatin to dabrafenib and trametinib for any within this group) to capture the prevalence of clones which expanded in related treatment groups and were likely to be found in the population. We then supplemented the above lists with clones which had more than 50 cells in at least one of the four samples from the corresponding sequential treatment group for each cDNA sample and also had at least one read in the gDNA sample. This ensured that we still analyzed clones that had grown out in one of the related treatment groups, even if it only had minimal gDNA representation. Finally, we subsetted these lists to contain only clones with at least 5 cells in each individual cDNA sample. These methods ensured that all resistant clones had some level of detection in both gDNA and cDNA barcode sequencing without filtering out important clones that were only highly detected in later treatment groups.

Analysis of transcriptional similarity based on treatment order

We grouped cells from samples that had survived 6.5-8 weeks of any combination of treatment based on whether they received a combination of dabrafenib and trametinib, $CoCl_2$, or cisplatin as either the first or second treatment. We then calculated pairwise Pearson correlations based on the scaled data generated in Seurat[65] of 2000 variable genes for all cells within the group. Additionally, we created random datasets matching the same number of cells for each experimental grouping of cells and calculated the pairwise Pearson correlations identically. We then performed two-tailed t-tests comparing the pairwise Pearson correlations of cells grouped by receiving a treatment as either their first or second treatment. We additionally compared each grouping of cells to the associated random dataset. We repeated this analysis in Figures S3A–S3C, omitting all cells that received the same treatment twice. For plotting violin plots of pairwise Pearson correlations, we subsampled 10,000,000 random data points.

Clone similarity analysis

We first identified resistant clones with at least five cells in each of the 12 treatment conditions (as described above). We then calculated the pairwise Pearson correlations in gene expression across the scale.data[65] of 2000 variable genes within the cells from each clone in each condition. Meanwhile, for each clone in each condition, we randomly sampled size-matched controls from cells that had survived the same treatment 100 times. For each simulation, we compared the average Pearson correlations of the real clones to those of the simulated clones using a one-sided Wilcoxon Rank Sum Test to test whether the correlation within the real clones were greater than the simulated clones. In Figure 4, the first simulation for each treatment condition is displayed.

Induced resistance computational analysis

To find clones with resistance that was induced to survive a treatment by first surviving a different treatment, we identified resistant clones within each treatment condition with a lenient filter of having more than one sequencing read in the barcodes sequenced from gDNA. The more lenient determination of whether a clone was resistant to a condition ensured that we accurately identified clones that had not survived a treatment from those that had survived a condition with only minimal growth such that it was not previously identified as resistant. We then generated lists of induced clones that only survived a treatment after developing resistance to a different treatment. We then mined these lists for clones which we had corresponding scRNA-seq data. We then used FindMarkers in the Seurat package[65] to identify genes up- or downregulated in induced clones compared to cells from clones that had survived the same initial treatment, but were not induced to survive the second treatment (Figures S6A, S6F, and S6G) with a logfc.threshold of 0.25 and p_val <= 0.05. We then performed directional gene set enrichment of the Molecular Signals Database (v2022.1) collection of hallmark gene sets[60,61] using the fgsea package (v1.22.0)[63] with a minSize of 5 and maxSize of 500 (Figures S6C, S6H, and S6I).

Gene ontology analysis

We used the FindMarkers method in Seurat[65] to create two lists of genes that increased or decreased between the four and 6.5–8 week time points in the same treatment. We input universally normalized Seurat objects (see STAR Methods section "scRNA-seq analysis"). We used default parameters for Seurat objects. We only listed genes with a minimum $\log_2$ fold change greater than 0.25 and that were expressed in at least 10% of cells. We added 1 to average expression values when $\log_2$ fold change was calculated. We input these lists into the enrichGO function in the clusterProfiler (v4.8.3)[33] library using default parameters and a p-value cutoff of 0.05. We used Bonferroni corrections to adjust p-values and only analyzed gene ontologies with q-values of 0.2 or less. Further, we only considered gene sets with a minimum of 10 genes and a maximum of 500 genes. We displayed gene ontologies that did not pass thresholds in grey and gene ontologies that went up in both directions as yellow. We determined "molecular function" gene ontologies. We plotted GO terms based on genes whose expression increased over time as the $-\log_{10}$(q-value) (resulting in positive values) and those based on genes whose expression decreased over time as the $\log_{10}$(q-value) (resulting in negative values). We analyzed resistant clones with five or more cells (as described above) at both time points using the same methodology as applied to whole populations to determine GO terms that had changed within individual clones.

Pathway variability analysis

To assess variability at the pathway level between clones and within clones, we quantified pathway activity at the single cell level for downstream quantification of variability. We used all GO-terms displayed in Figures 6B–6E and S7 and extracted their gene lists. We then calculated single-cell pathway scores for each GO-term using the UCell (v2.4.0)[42] package in R. For subsequent analyses, we only included barcoded clones containing five or more cells at both the first and second time point. To quantify interclonal variation (between clones), we calculated the mean UCell score per clone and then the coefficient of variation across the clones (Figures S9A and S9B). To quantify intraclonal variation (within the clone), we calculated the coefficient of variation on the UCell scores for each cell (Figures S9C and S9D).

Computational analysis of induced resistance validation

We used custom python scripts to count the number of pixels that were covered by nuclei in each image to measure survival in the dish. In brief, we cropped the images to include only the inside of the well in each square image. We then used the scikit-image (v0.21.0)[64] package to perform gaussian filtering, median filtering, and then Niblack thresholding to establish local thresholds for areas covered by cells. We binarized these images, converting any pixel where the fluorescence was greater than the local threshold * 1.01 to be part of a cell (equal to 1) and other pixels to background (equal to 0). We then used scikit-image to remove objects smaller than 64 pixels to remove small patches of background pixels that passed thresholding. Finally, we removed the outer ring of pixels in the image that were above threshold due to edge effects and output the total number of filtered pixels above threshold for further processing. We visually inspected these images to ensure that the resulting binarized images were accurately reflecting the areas in which cells were located on the dish and thus estimating the cell number. This workflow allowed robust quantification even when it was not possible to accurately segment cell nuclei in highly confluent resistant clones that have lost contact inhibition.

In a custom R script, we calculated the average area (in pixels) covered by cells per well. For the first biological replicate (Figure S6D), we plotted the $\log_2$ of the number of pixels and performed a one-sided t-test to evaluate whether IL6ST-high cells had improved growth in $CoCl_2$ compared to IL6ST-low cells. For the second biological replicate (Figure S6E), which included a plating control to account for counting errors between the IL6ST-high and low samples, we normalized the total pixel area in the treated wells by the average pixel area of the corresponding control wells (fixed immediately after the plated cells adhered). Using these plating-normalized areas, we plotted IL6ST level versus the log-two of the normalized cell area and performed a one-sided t-test on the normalized area to determine p-values.

Computational analysis of clone abundance during continued treatment of *EGFR*- and *NGFR*-high dabrafenib and trametinib resistant clones

To assess how prolonged combination treatment with dabrafenib and trametinib affected clones with high *EGFR* or *NGFR* expression, we began by clustering the cells sequenced after four and 6.5 weeks of dabrafenib treatment together and forced Seurat to cluster these cells into only two subclusters using FindClusters with a resolution of 0.015. Based on gene expression plots, we identified one cluster as *EGFR*-high and one cluster as *NGFR*-high, noting that both clusters contained cells from each duration of treatment. We then identified 44 resistant clones with at least five cells (as defined above) after four weeks of treatment with dabrafenib and trametinib. We then calculated the percentage of cells from each resistant clone that were in the *EGFR*- or *NGFR*-high cluster. We then followed these same 44 clones through to the 6.5 week treatment sample and identified whether a clone died (defined as no longer being identified as a resistance clone as defined above) and calculated the percentage of each surviving clone in each cluster. We then more broadly assessed the survival of the clones by counting how many cells from each of the 44 clones were present in each of the three samples that had received a secondary round of treatment (dabrafenib and trametinib to dabrafenib and trametinib, dabrafenib and trametinib to $CoCl_2$, and dabrafenib and trametinib to cisplatin).

We used the escape package (v1.8.0)[66] to calculate single-cell UCell enrichment scores for cells from *EGFR*-high, *NGFR*-high, and mixed clones using the melanocytic, neural crest-like, transitory, and undifferentiated gene sets from Tsoi et al.[47] We compared the expression of these gene states between conditions using an ANOVA followed by Tukey's honest significant difference tests.

Computational analysis of EGFR and NGFR HCR RNA FISH

We used Nimbus Image to analyze the HCR FISH data (https://github.com/Kitware/UPennContrast and https://github.com/arjunrajlaboratory/ImageAnalysisProject/). First, we contrasted DAPI and HCR signal. We then used the DAPI signal to guide manual circling of individual clone masks. We then annotated each clone as either predominantly *EGFR*-high, predominantly *NGFR*-high, clones with evenly mixed expression, and clones that were too ambiguous to classify. Next, we measured the total DAPI expression within each circled clone mask along with the coordinates of their centroids. Finally, we exported low resolution snapshots of the images including the masks that were traced, colored, and overlaid on high resolution images in Adobe Illustrator for Figures 7C and S11A–S11C along with scale bars that were made in ImageJ.[62]

ADDITIONAL RESOURCES

Barcode Library

We performed DNA barcoding with the Rewind library using barcode plasmids provided generously by the Raj Lab at the University of Pennsylvania and produced as previously described.[26] Briefly, PAGE-purified Ultramer oligonucleotides were ordered containing a 100-base pair sequence repeating 'WSN', where W = A or T, S = G or C, and N = any base pair, and inserted into a lentivirus vector backbone downstream of the EFS promoter and GFP sequence. Emert et al. have published a detailed protocol of how these barcodes are produced (https://www.protocols.io/view/barcode-plasmid-library-cloning-5qpvon6yxl4o/v1),[26] and the plasmid sequence is available (https://benchling.com/shaffer_lab/f/lib_6JXLhfQH-plasmids/seq_BUIxqCk0-lentiefs_gfp_100bp_barcode_v1/edit?m=slm-GJ609ijArVWmkT8mk8zr).[11]

Cell Systems, Volume *15*

Supplemental information

Clonal differences underlie variable responses to sequential and prolonged treatment

Dylan L. Schaff, Aria J. Fasse, Phoebe E. White, Robert J. Vander Velde, and Sydney M. Shaffer

Supplemental Information

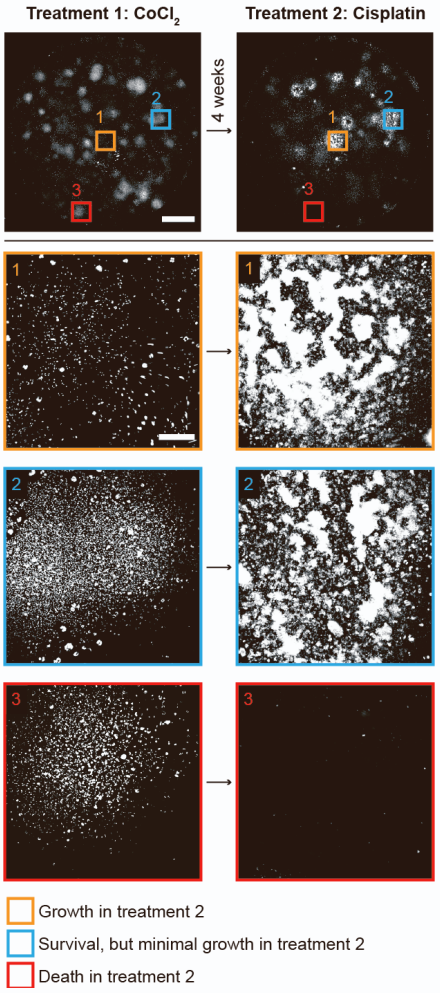

Supplemental Figure 1: Cancer cell clones exhibit variable responses to first and second treatments. (Top) WM989 BRAF V600E mutant melanoma cells with a nuclear GFP tag imaged after four weeks in $CoCl_2$ followed by four weeks in cisplatin. Below are cropped images from the whole well scans showing clones that grew (orange), survived with low growth (blue), or mostly died (red) in the second treatment. Cisplatin resistant cells tend to grow on top of each other causing cropped images to look out of focus. Scale bars in whole well scans are 5 mm while scale bars in cropped scans are 500 μm and apply to all cropped scans.

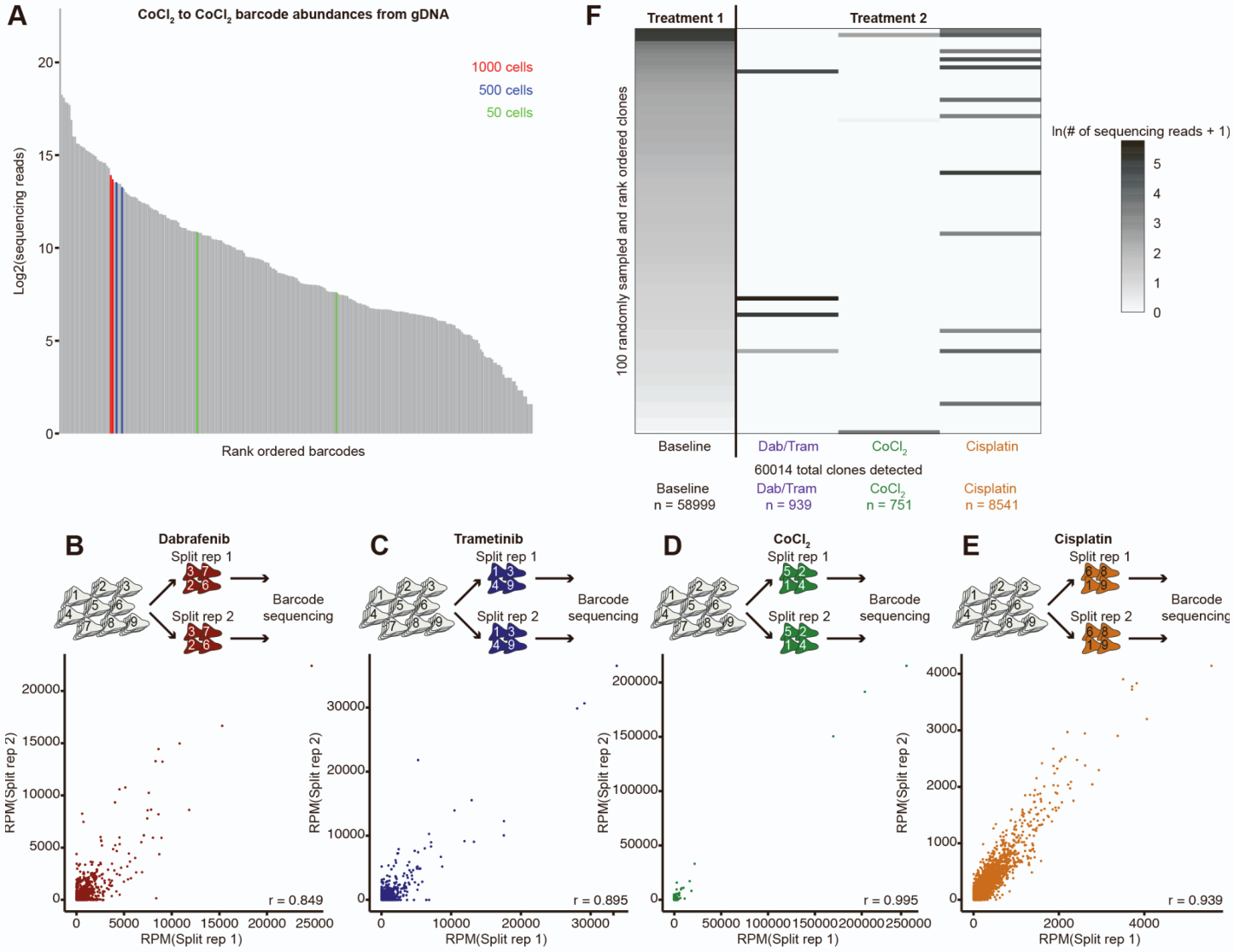

Supplemental Figure 2: Clonal barcode reads are a quantitative readout for cell number. A) Sequencing reads of DNA barcodes from gDNA using the $CoCl_2$ to $CoCl_2$ condition as an example. Displayed are the log_2(# of sequencing reads) with the ladder barcodes highlighted in red (1000 cells), blue (500 cells), and green (50 cells). Only barcodes with at least two reads are displayed. **B-E)** Scatter plots showing barcode abundance from experiments testing the heritability of resistance phenotypes in dabrafenib, trametinib, $CoCl_2$, and cisplatin. We transduced melanoma cells with barcodes, allowed them to go through 6 doublings, then split these into two separate samples per treatment (labeled as split rep 1 and 2 in figure). We applied each of the different treatments and then quantified cell survival and proliferation by sequencing the barcodes in each sample. Scatter plots show the Reads Per Million (RPM) normalized reads for each barcode across the two samples. A high Pearson correlation in the barcode reads indicates that the same barcoded clones are surviving and proliferating in each sample. **F)** Heatmaps showing 100 randomly sampled and rank-ordered clones immediately prior to treatment being applied (baseline) followed by their abundance after initial treatment with a combination of dabrafenib and trametinib (Dab/Tram), $CoCl_2$, and cisplatin. Individual clones are colored by the ln(Reads Per Million (RPM) + 1) using data from sequencing clonal barcodes from gDNA of surviving cells. It should be noted that there are clones whose abundance were below the threshold of detection in the pretreatment sample, but were detected after the first round of treatment. The total number of unique clones that were detected before or after initial treatment is displayed below the heatmap, followed by the number of clones detected after each treatment.

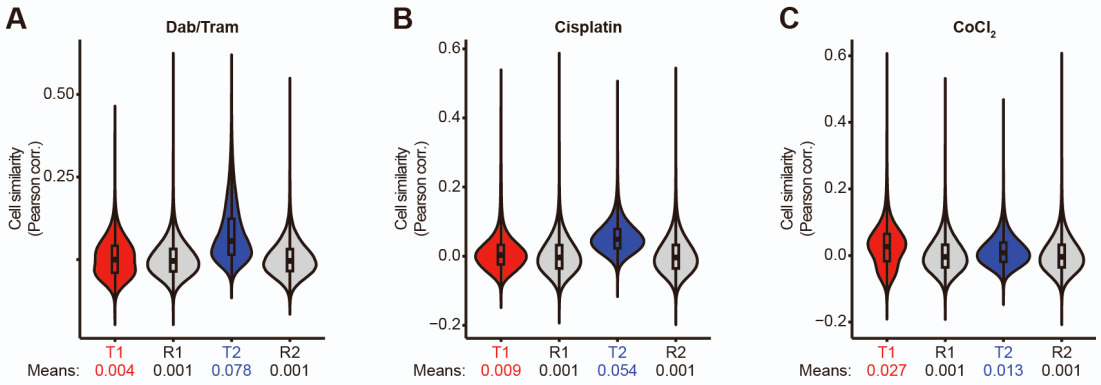

Supplemental Figure 3: Same analysis as Figure 3B while excluding samples that received the same treatment twice. Displayed is the quantification of cell similarity using pairwise Pearson correlations of gene expression (top 2000 most variable genes). **A)** For dabrafenib and trametinib (Dab/Tram), pairwise Pearson correlations between cells that received Dab/Tram first (T1) were ~3.0-fold higher than the matched random sampling of cells (R1), while correlations between cells that received Dab/Tram second (T2) were ~55-fold higher than the matched control (R2) and ~20-fold higher than those that received Dab/Tram first. **B)** For cisplatin treatment, pairwise Pearson correlations between cells that received cisplatin first were ~6.5-fold higher than the matched random sampling of cells, while correlations between cells that received cisplatin second were ~40-fold higher than the matched control and ~6.1-fold higher than those that received cisplatin first. **C)** For $CoCl_2$ treatment, pairwise Pearson correlations between cells that received $CoCl_2$ first were ~20-fold higher than the matched random sampling of cells and ~2.2 fold higher than those that received $CoCl_2$ second, while correlations between cells that received $CoCl_2$ second was ~9.4-fold greater than the matched random control. All comparisons were statistically significant by a two-sided t-test with $p < 2.2e\text{-}16$. Violin plots display 10,000,000 subsampled data points per condition, but statistical comparisons and averages were calculated on non-subsampled data. Mean values are displayed below each graph.

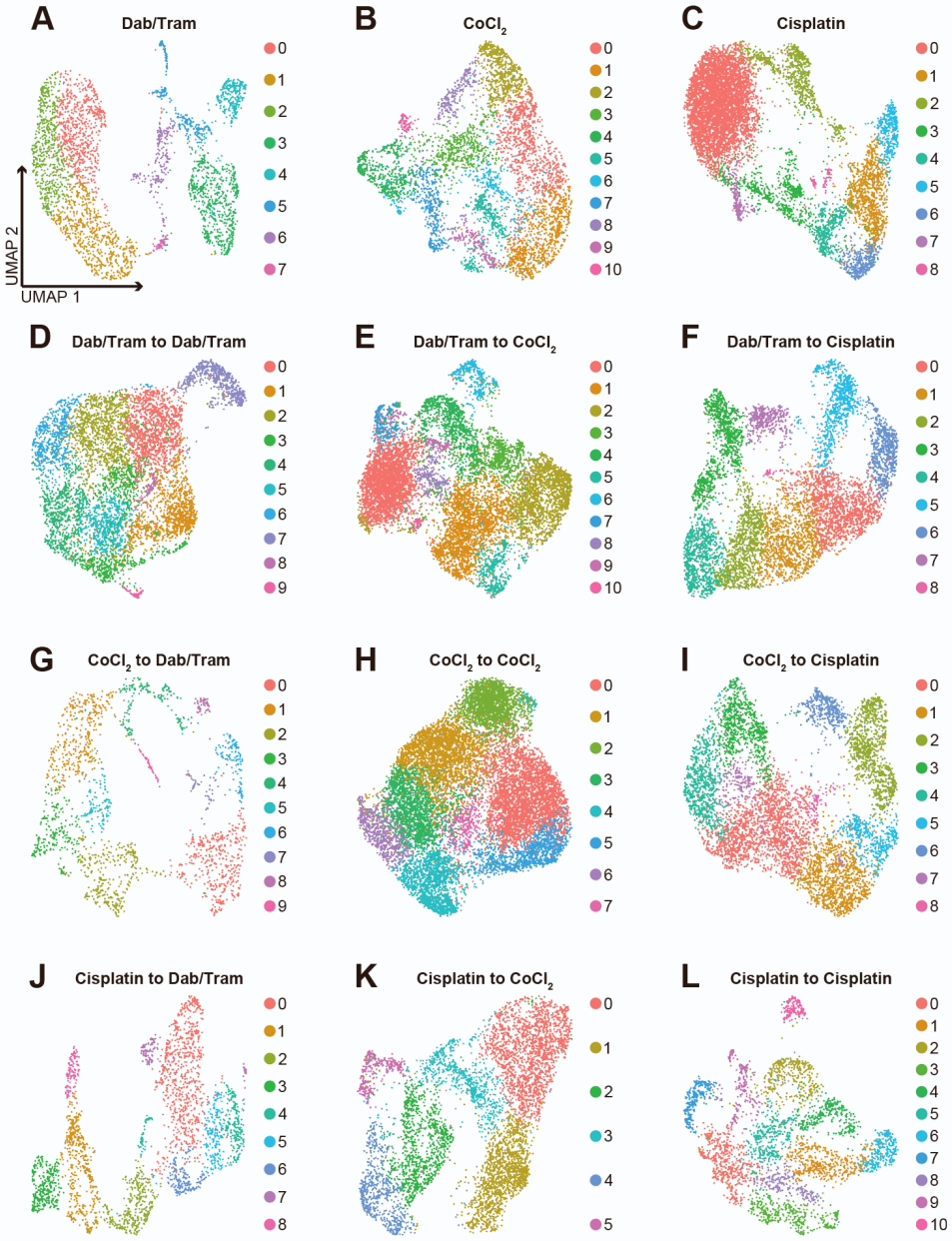

Supplemental Figure 4: UMAPs of each condition individually. UMAP (GEO: GSE253739) projections of **A)** dabrafenib and trametinib (Dab/Tram, 3203 cells), **B)** $CoCl_2$ (4823 cells), **C)** cisplatin (8303 cells), **D)** Dab/Tram to Dab/Tram (6906 cells), **E)** Dab/Tram to $CoCl_2$ (10184 cells), **F)** Dab/Tram to cisplatin (7070 cells), **G)** $CoCl_2$ to Dab/Tram (1773 cells), **H)** $CoCl_2$ to $CoCl_2$ (13951 cells), **I)** $CoCl_2$ to cisplatin (6459 cells), **J)** cisplatin to Dab/Tram (2615 cells), **K)** cisplatin to $CoCl_2$ (5715 cells), and **L)** cisplatin to cisplatin (3323 cells) treated cells. The UMAP projections are colored based on their default Seurat[65] clustering.

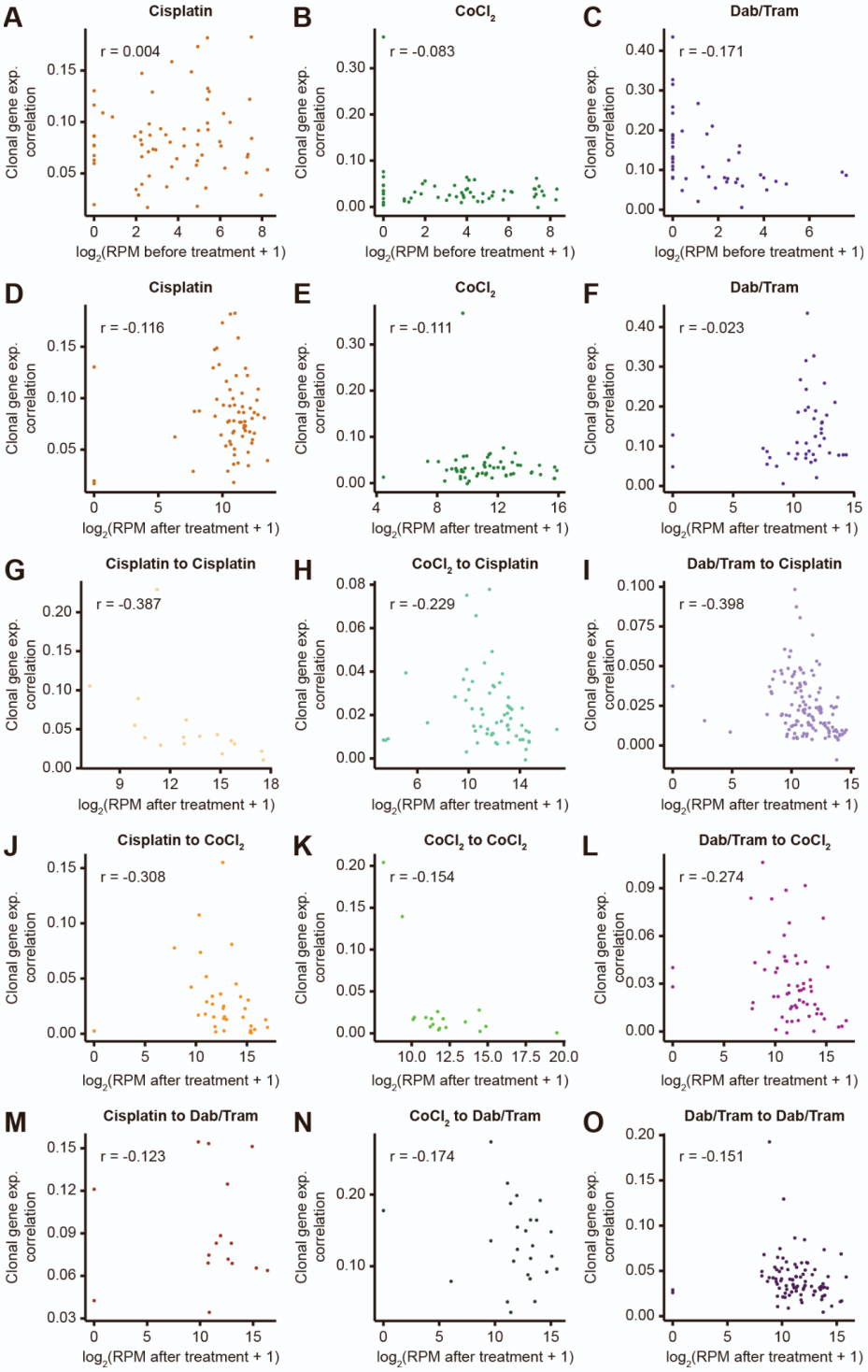

Supplemental Figure 5: Comparing clonal gene expression similarity to size before and after treatment. A-C) We compared the average pairwise Pearson gene expression correlation (top 2000 most variable genes) of all clones where we detected at least five cells by scRNA-seq after initial treatment with their abundance in the gDNA sample collected prior to treatment. **D-F)** We compared the same clones that have survived one of the three initial treatments with their size in the gDNA samples collected after initial treatment. **G-O)** We compared clones that had survived two rounds of treatment (five or more cells detected by scRNA-seq) with their size in the gDNA samples collected after two rounds of treatment. In all subpanels, Pearson correlations between gene expression correlation and clone size are displayed as r = #.

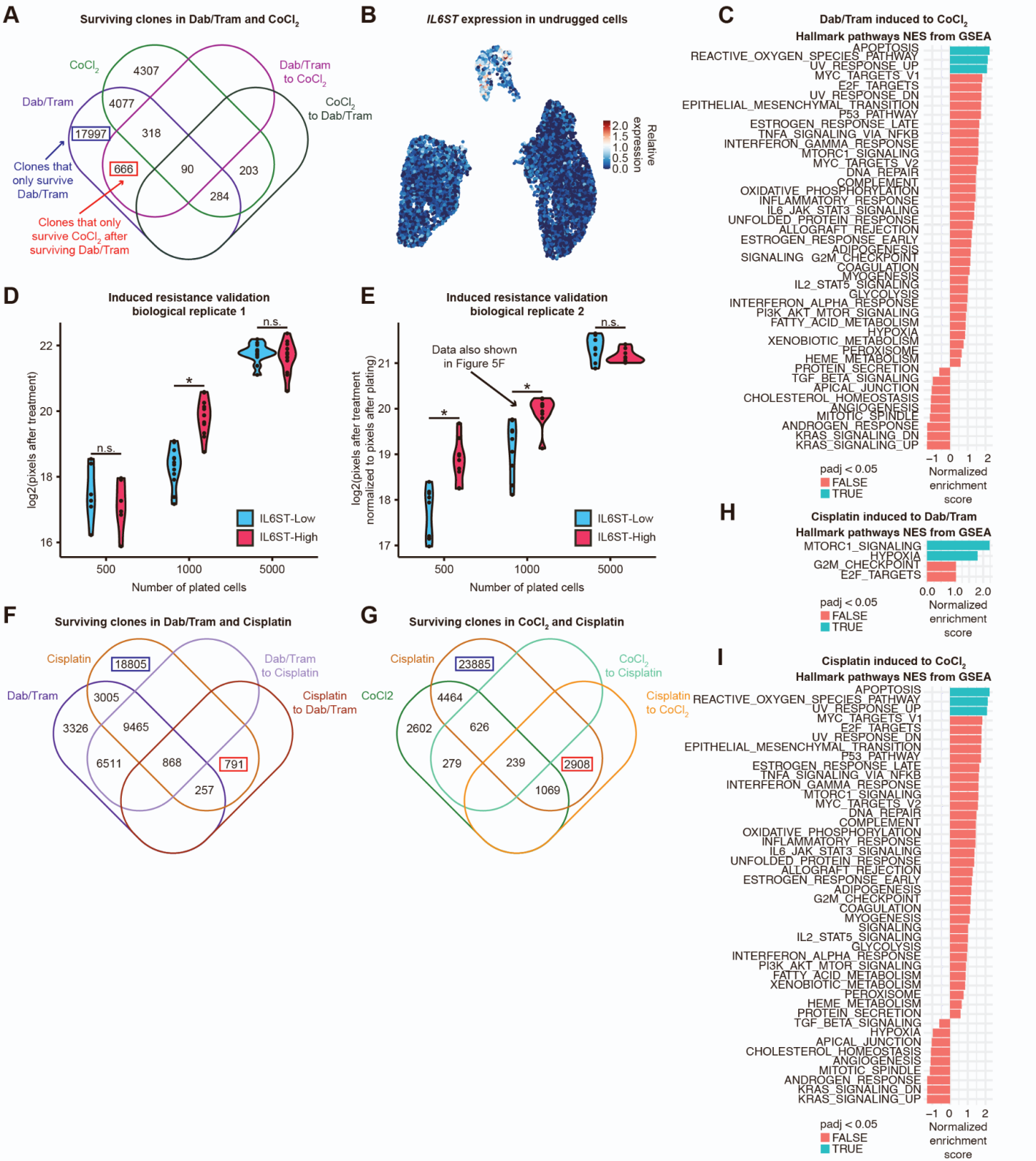

Supplemental Figure 6: Treatment can induce resistance to a second therapy in otherwise sensitive clones. A) Venn diagram comparing clones that survived dabrafenib and trametinib (Dab/Tram), $CoCl_2$, Dab/Tram to $CoCl_2$, and $CoCl_2$ to Dab/Tram. Boxed in red are the 666 clones that only survived $CoCl_2$ after previous treatment with Dab/Tram. Boxed in blue are the 17997 clones that survived Dab/Tram but were still sensitive to $CoCl_2$. **B)** UMAP of scRNA-seq data displaying the relative *IL6ST* expression in untreated cells from Harmange et al.[11] (GEO: GSE237228). The color scale describes log-normalized data. **C)** We identified genes differentially expressed between clones boxed in blue and red in **A** to find pathways enriched and

depleted in clones that were induced to survive $CoCl_2$ by Dab/Tram. All pathways displayed were significantly enriched ($p < 0.05$), the blue bars indicate that the adjusted p-value was also < 0.05. **D)** Induced resistance validation biological replicate 1. The log2(number of pixels covered by cells) were compared at each number of cells plated: 500, 1000, and 5000. IL6ST-high, dabrafenib and trametinib resistant cells had more survival in $CoCl_2$ than IL6ST-low cells when seeded at 1000 cells per well as determined by a one-sided t-test with $p < 5x10^{-5}$. Other comparisons were not significant (n.s.). Experimental schematic shown in Figure 5D. **E)** Induced resistance validation biological replicate 2. These data were normalized to plates fixed the day after plating to account for potential variation in plating. The log2(normalized number of pixels covered by cells) were compared at each number of cells plated: 500, 1000, and 5000. IL6ST-high, dabrafenib and trametinib resistant cells had more survival in $CoCl_2$ than IL6ST-low cells when seeded at 500 ($p < 5x10^{-3}$) and 1000 ($p < 5x10^{-4}$) cells per well as determined by a one-sided t-test. Other comparisons were not significant (n.s.). Experimental schematic shown in Figure 5D. The data for the 1000 cells per well seeding is also displayed in Figure 5F. **F)** Venn diagram comparing clones that survived Dab/Tram, cisplatin, Dab/Tram to cisplatin, and cisplatin to Dab/Tram. Boxed in red are the 791 clones that only survived Dab/Tram after previous treatment with cisplatin. Boxed in blue are the 18805 clones that survived cisplatin but were still sensitive to Dab/Tram. **G)** Venn diagram comparing clones that survived $CoCl_2$, cisplatin, $CoCl_2$ to cisplatin, and cisplatin to $CoCl_2$. Boxed in red are the 2908 clones that only ever survived Dab/Tram after previous treatment with cisplatin. Boxed in blue are the 23885 clones that survived cisplatin but were still sensitive to Dab/Tram. **H)** Differentially expressed pathways in clones with resistance to Dab/Tram induced by cisplatin. All pathways displayed were significantly enriched ($p < 0.05$), the blue bars indicate that the adjusted p-value was also < 0.05. **I)** Differentially expressed pathways in clones with resistance to $CoCl_2$ induced by cisplatin. All pathways displayed were significantly enriched ($p < 0.05$), the blue bars indicate that the adjusted p-value was also < 0.05.

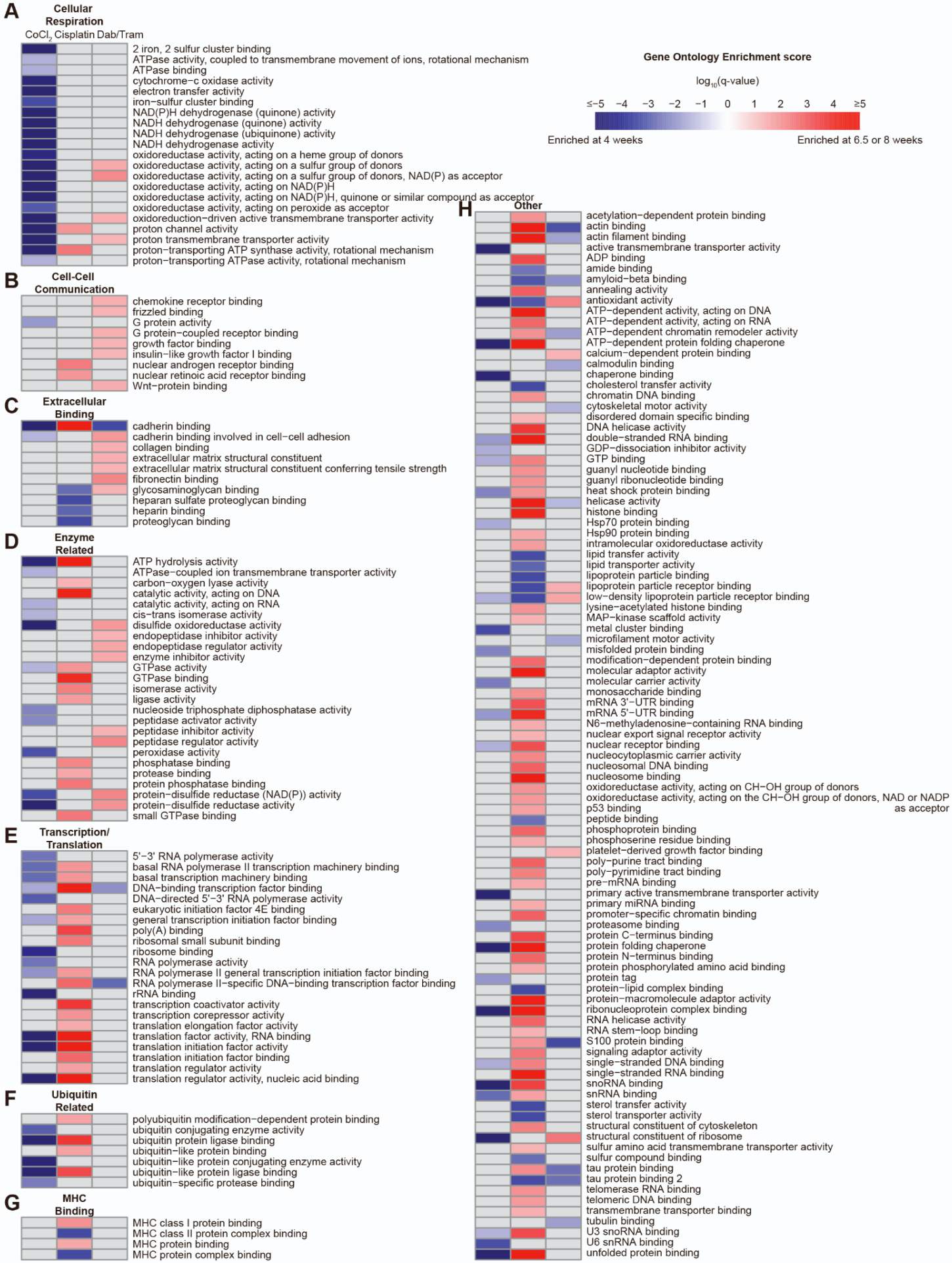
A
Cellular Respiration
$CoCl_2$ Cisplatin Dab/Tram
2 iron, 2 sulfur cluster binding
ATPase activity, coupled to transmembrane movement of ions, rotational mechanism
ATPase binding
cytochrome−c oxidase activity
electron transfer activity
iron−sulfur cluster binding
NAD(P)H dehydrogenase (quinone) activity
NADH dehydrogenase (quinone) activity
NADH dehydrogenase (ubiquinone) activity
NADH dehydrogenase activity
oxidoreductase activity, acting on a heme group of donors
oxidoreductase activity, acting on a sulfur group of donors
oxidoreductase activity, acting on a sulfur group of donors, NAD(P) as acceptor
oxidoreductase activity, acting on NAD(P)H
oxidoreductase activity, acting on NAD(P)H, quinone or similar compound as acceptor
oxidoreductase activity, acting on peroxide as acceptor
oxidoreduction−driven active transmembrane transporter activity
proton channel activity
proton transmembrane transporter activity
proton−transporting ATP synthase activity, rotational mechanism
proton−transporting ATPase activity, rotational mechanism
B
Cell-Cell Communication
chemokine receptor binding
frizzled binding
G protein activity
G protein−coupled receptor binding
growth factor binding
insulin−like growth factor I binding
nuclear androgen receptor binding
nuclear retinoic acid receptor binding
Wnt−protein binding
C
Extracellular Binding
cadherin binding
cadherin binding involved in cell−cell adhesion
collagen binding
extracellular matrix structural constituent
extracellular matrix structural constituent conferring tensile strength
fibronectin binding
glycosaminoglycan binding
heparan sulfate proteoglycan binding
heparin binding
proteoglycan binding
D
Enzyme Related
ATP hydrolysis activity
ATPase−coupled ion transmembrane transporter activity
carbon−oxygen lyase activity
catalytic activity, acting on DNA
catalytic activity, acting on RNA
cis−trans isomerase activity
disulfide oxidoreductase activity
endopeptidase inhibitor activity
endopeptidase regulator activity
enzyme inhibitor activity
GTPase activity
GTPase binding
isomerase activity
ligase activity
nucleoside triphosphate diphosphatase activity
peptidase activator activity
peptidase inhibitor activity
peptidase regulator activity
peroxidase activity
phosphatase binding
protease binding
protein phosphatase binding
protein−disulfide reductase (NAD(P)) activity
protein−disulfide reductase activity
small GTPase binding
E
Transcription/ Translation
5′−3′ RNA polymerase activity
basal RNA polymerase II transcription machinery binding
basal transcription machinery binding
DNA−binding transcription factor binding
DNA−directed 5′−3′ RNA polymerase activity
eukaryotic initiation factor 4E binding
general transcription initiation factor binding
poly(A) binding
ribosomal small subunit binding
ribosome binding
RNA polymerase activity
RNA polymerase II general transcription initiation factor binding
RNA polymerase II−specific DNA−binding transcription factor binding
rRNA binding
transcription coactivator activity
transcription corepressor activity
translation elongation factor activity
translation factor activity, RNA binding
translation initiation factor activity
translation initiation factor binding
translation regulator activity
translation regulator activity, nucleic acid binding
F
Ubiquitin Related
polyubiquitin modification−dependent protein binding
ubiquitin conjugating enzyme activity
ubiquitin protein ligase binding
ubiquitin−like protein binding
ubiquitin−like protein conjugating enzyme activity
ubiquitin−like protein ligase binding
ubiquitin−specific protease binding
G
MHC Binding
MHC class I protein binding
MHC class II protein complex binding
MHC protein binding
MHC protein complex binding
Gene Ontology Enrichment score
$\log_{10}$(q-value)
≤−5 −4 −3 −2 −1 0 1 2 3 4 ≥5
Enriched at 4 weeks
Enriched at 6.5 or 8 weeks
H
Other
acetylation−dependent protein binding
actin binding
actin filament binding
active transmembrane transporter activity
ADP binding
amide binding
amyloid−beta binding
annealing activity
antioxidant activity
ATP−dependent activity, acting on DNA
ATP−dependent activity, acting on RNA
ATP−dependent chromatin remodeler activity
ATP−dependent protein folding chaperone
calcium−dependent protein binding
calmodulin binding
chaperone binding
cholesterol transfer activity
chromatin DNA binding
cytoskeletal motor activity
disordered domain specific binding
DNA helicase activity
double−stranded RNA binding
GDP−dissociation inhibitor activity
GTP binding
guanyl nucleotide binding
guanyl ribonucleotide binding
heat shock protein binding
helicase activity
histone binding
Hsp70 protein binding
Hsp90 protein binding
intramolecular oxidoreductase activity
lipid transfer activity
lipid transporter activity
lipoprotein particle binding
lipoprotein particle receptor binding
low−density lipoprotein particle receptor binding
lysine−acetylated histone binding
MAP−kinase scaffold activity
metal cluster binding
microfilament motor activity
misfolded protein binding
modification−dependent protein binding
molecular adaptor activity
molecular carrier activity
monosaccharide binding
mRNA 3′−UTR binding
mRNA 5′−UTR binding
N6−methyladenosine−containing RNA binding
nuclear export signal receptor activity
nuclear receptor binding
nucleocytoplasmic carrier activity
nucleosomal DNA binding
nucleosome binding
oxidoreductase activity, acting on CH−OH group of donors
oxidoreductase activity, acting on the CH−OH group of donors, NAD or NADP as acceptor
p53 binding
peptide binding
phosphoprotein binding
phosphoserine residue binding
platelet−derived growth factor binding
poly−purine tract binding
poly−pyrimidine tract binding
pre−mRNA binding
primary active transmembrane transporter activity
primary miRNA binding
promoter−specific chromatin binding
proteasome binding
protein C−terminus binding
protein folding chaperone
protein N−terminus binding
protein phosphorylated amino acid binding
protein tag
protein−lipid complex binding
protein−macromolecule adaptor activity
ribonucleoprotein complex binding
RNA helicase activity
RNA stem−loop binding
S100 protein binding
signaling adaptor activity
single−stranded DNA binding
single−stranded RNA binding
snoRNA binding
snRNA binding
sterol transfer activity
sterol transporter activity
structural constituent of cytoskeleton
structural constituent of ribosome
sulfur amino acid transmembrane transporter activity
sulfur compound binding
tau protein binding
tau protein binding 2
telomerase RNA binding
telomeric DNA binding
transmembrane transporter binding
tubulin binding
U3 snoRNA binding
U6 snRNA binding
unfolded protein binding

Supplemental Figure 7: Gene Ontology comparing cells in the same agent after first and second treatment. We compared cells from the same agent after the first and second round of treatment, identifying differentially expressed genes between the two. We then identified GO terms enriched after either the first round of treatment (four weeks, blue) or after the second round of treatment (6.5 or eight weeks, red) based on the $\log_{10}$(q-value) and -$\log_{10}$(q-value) respectively. GO terms that were not significantly enriched, or failed other thresholds, in either direction for a condition are colored in grey. Subpanels **A-G** show the same pathways in the same order as in Figure 6B, showing the pathways that make up each category. **H)** The “other” category includes all of the pathways that were significant in at least one of the three comparisons that we did not group into one of the seven other categories. Column labels indicate the agent from which cells after the first and second round of treatment were compared.

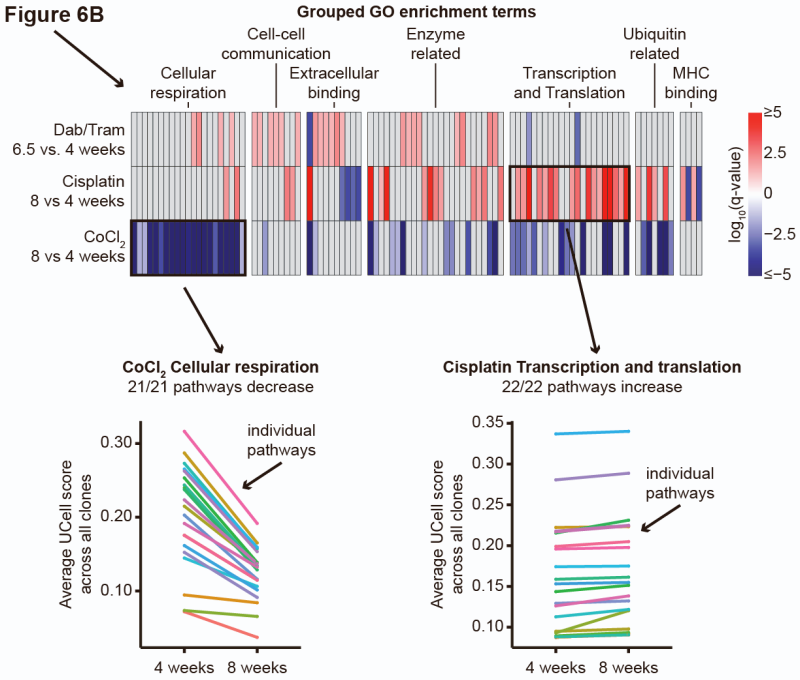

Supplemental Figure 8: Changes in UCell scoring of pathway activity show similar trends to GO enrichment over time. (Top) Figure 6B highlighting cellular respiration in $CoCl_2$ treatment and transcription and translation in cisplatin treatment. The color scale shows the $\log_{10}$(q-value) of directional enrichment. (Bottom left) The average UCell score across all $CoCl_2$-resistant clones (at least five cells detected by scRNA-seq at both timepoints) for cellular respiration is shown at four weeks and eight weeks for the 21 GO terms analyzed. The UCell score for all 21 pathways decreased over time which mirrored the global decrease in enrichment in Figure 6B. (Bottom right) The average UCell score across all cisplatin-resistant clones (at least five cells detected by scRNA-seq at both timepoints) for transcription and translation is shown at four weeks and eight weeks for the 22 GO terms analyzed. The UCell score for all 22 pathways increased over time which mirrored the increases in enrichment in Figure 6B.

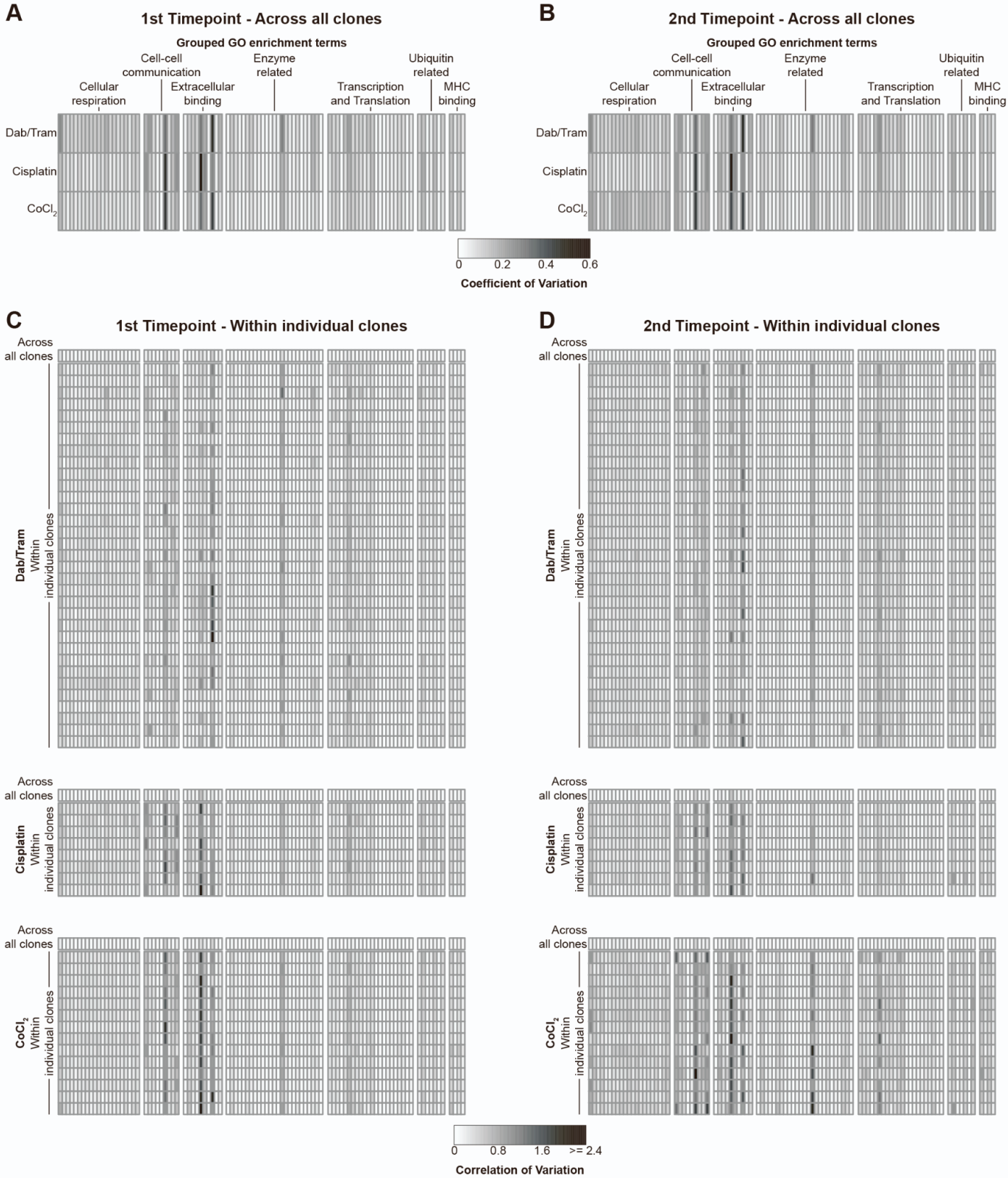

Supplemental Figure 9: Quantification of pathway variability across (interclonal) and within clones (intraclonal). A,B) Heatmaps displaying coefficients of variations across clones calculated using the average UCell enrichment score for each clone detected within a treatment. The left plot **(A)** is after four weeks of treatment. The right plot **(B)** is after 6.5 weeks (dabrafenib and trametinib, Dab/Tram) or eight weeks (cisplatin and $CoCl_2$) of treatment. Color scale legend for the coefficient of variation is shown in white (0) to black (0.6). **C,D)** Heatmaps displaying coefficients of variations within clones calculated using the UCell enrichment scores of every cell within resistant clones. Left plots (**C**) are after four weeks of treatment. Right plots **(D)** are after 6.5

(Dab/Tram) or eight weeks (cisplatin and $CoCl_2$) of treatment. The top row for each condition displays the variation across clones from **A** and **B**. Color scale legend for the coefficient of variation is shown in white (0) to black (>=2.4). Color scales used in **A** and **B** are different from color scales used in **C** and **D** such that the differences are visible. Both color scales are linear.

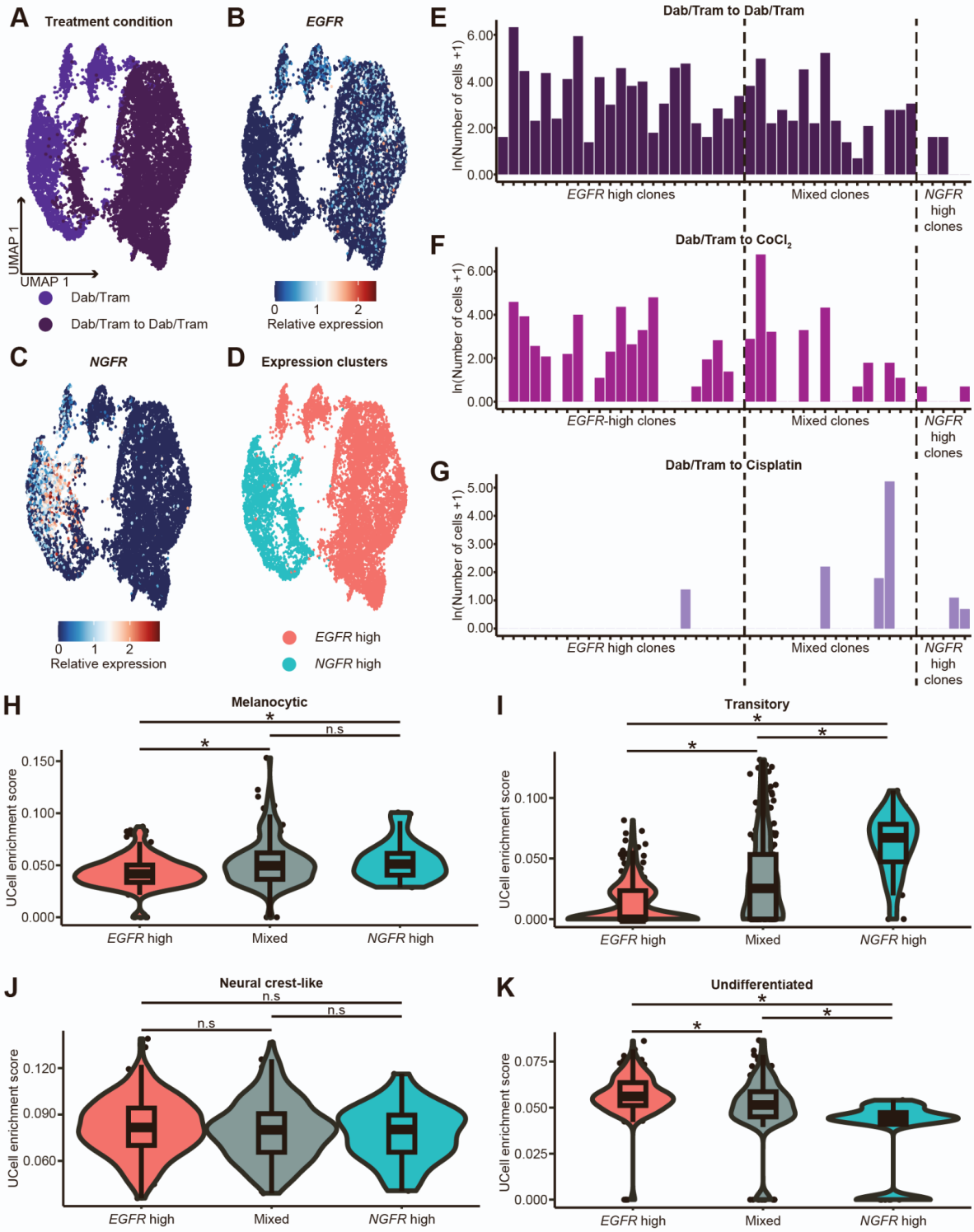

Supplemental Figure 10: Dabrafenib and trametinib treated cells enter either an *EGFR*- or *NGFR*-high state. A) UMAP (GEO: GSE253739) projection of cells that have only been treated with dabrafenib and trametinib (Dab/Tram) after the first (four weeks) and second (6.5 weeks) rounds of treatment. The cells cluster predominantly by condition, but also have overlap between conditions. Relative expression of **B)** *EGFR* or **C)** *NGFR*. Color scales are of log-normalized data. Cells expressing these markers are largely mutually exclusive. **D)** We constrained Seurat clustering to only allow two total clusters[65]. We denoted these clusters as *EGFR*-high and *NGFR*-high based on their correlation with the markers. We identified clones with at least five cells after initial Dab/Tram treatment and classified them as *EGFR*-high, mixed clones, and *NGFR*-high. We then measured the number of sequenced single-cells from these clones after secondary treatment with **E)** Dab/Tram, **F)** $CoCl_2$, **G)** and cisplatin treatment, displayed as ln(# of cells + 1). UCell scores from cells from

EGFR-high, *NGFR*-high, and mixed clones based on **H)** melanocytic, **I)** transitory, **J)** neural crest-like, and **K)** undifferentiated gene sets defined by Tsoi et al.[47]. * is p value < 0.05 by ANOVA followed by Tukey's honest significance difference test.

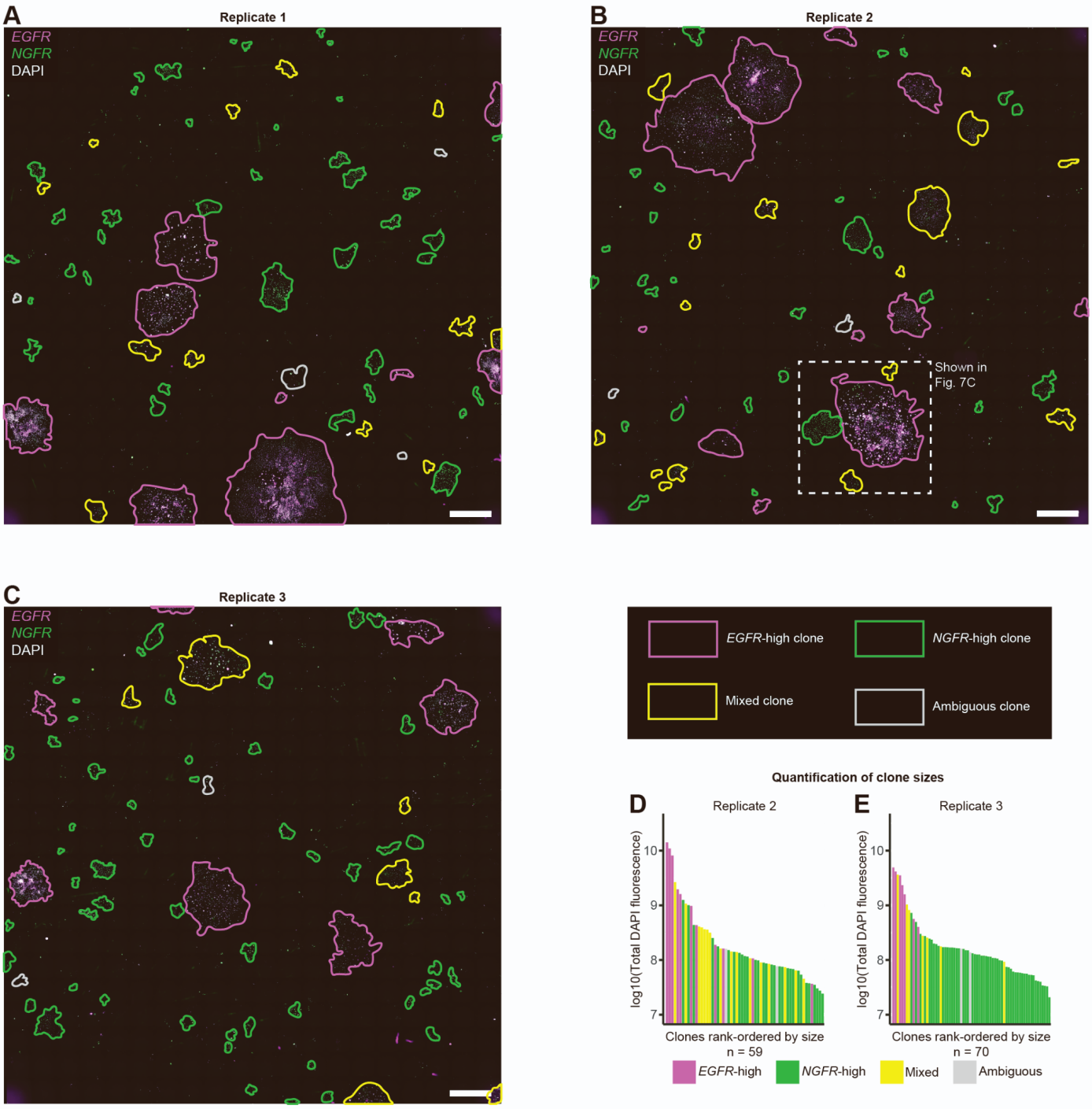

Supplemental Figure 11: Hybridization Chain Reaction of dabrafenib and trametinib resistant clones. A-C) Resistant clones were generated by treating WM989 A6-G3 melanoma cells with dabrafenib and trametinib for 6.5 weeks. We used Hybridization Chain Reaction (HCR) to label individual *EGFR* (magenta spots) and *NGFR* (green spots) transcripts within cells. Cell nuclei were stained with DAPI (grey). We then circled clones and classified them as predominantly *EGFR*-high (magenta), predominantly *NGFR*-high (green), mixed (yellow), or ambiguous (grey). In **B**, the dotted line outlines the region of replicate 2 displayed in Figure 7C. Scale bars are 2 mm. **D-E)** Quantification of clone sizes based on total DAPI fluorescence within circled clones from **B** (Replicate 2) and **C** (Replicate 3). Data is rank-ordered based on clone size and clones are colored based on their classification: *EGFR*-high, *NGFR*-high, mixed, or ambiguous.

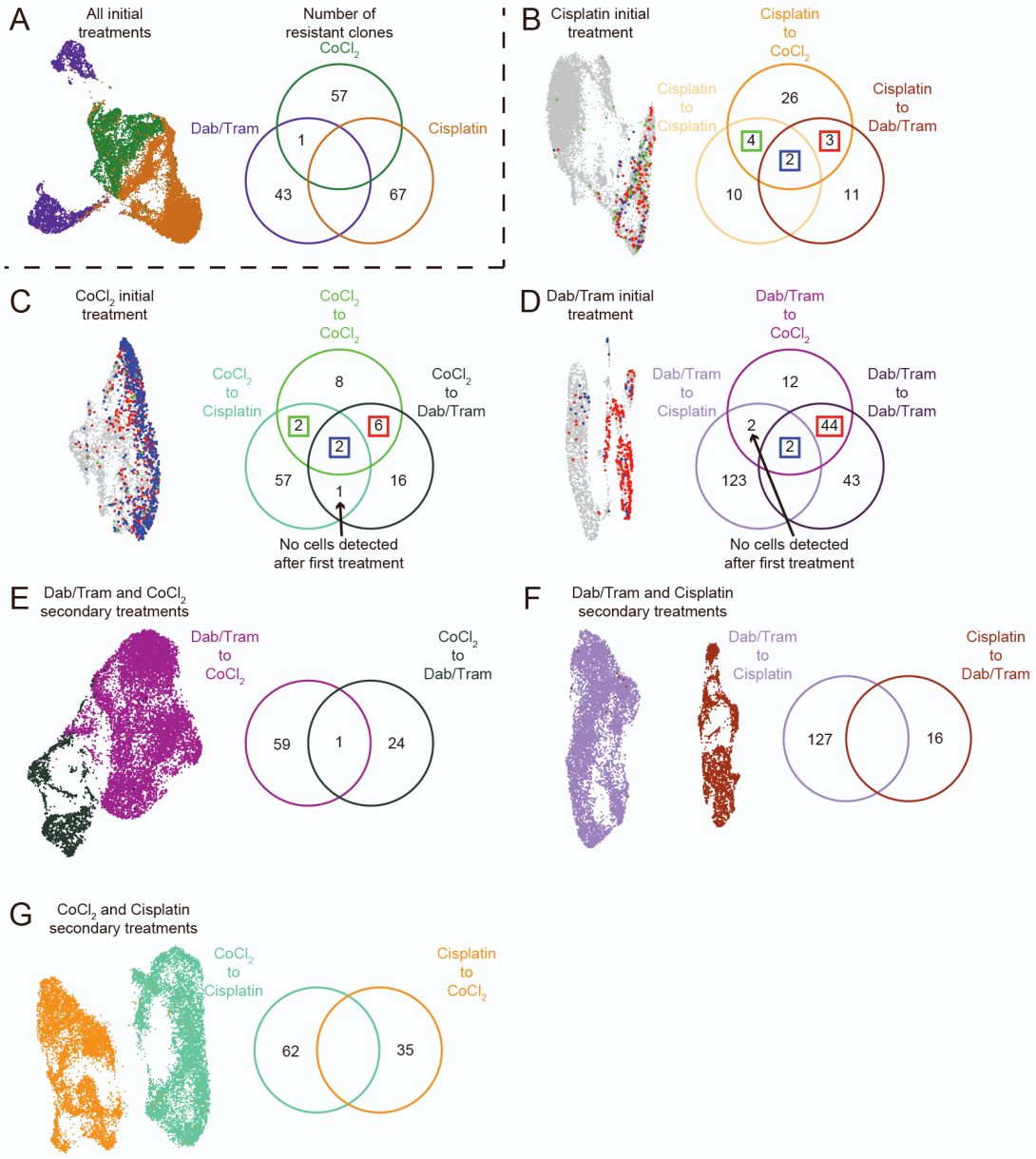

Supplemental Figure 12: Extreme subsampling prevents tracing individual clones through multiple rounds of treatment. A) (Left) UMAP (GEO: GSE253739) displays cells from the three samples that only received one treatment. Cells are colored by the treatment received. (Right) Venn diagram of clones resistant (with at least five cells detected by scRNA-seq) to each initial treatment. Only one clone survived more than one initial treatment. **B)** (Left) UMAP of the cells that only received cisplatin as an initial treatment. (Right) Venn diagram of clones resistant to each secondary treatment after initial treatment with cisplatin. The number of clones that survived multiple secondary treatments are boxed in either green, blue, or red. Cells from these clones are colored on the UMAP (left). The remaining cells are left grey. **C)** (Left) UMAP of the cells that only received $CoCl_2$ as an initial treatment. (Right) Venn diagram of clones resistant to each secondary treatment after initial treatment with $CoCl_2$. The number of clones that survived multiple secondary treatments are boxed in either green, blue, or red. Cells from these clones are colored on the UMAP (left). The remaining cells are left grey. An arrow indicates a condition where clones were identified as resistant to a second treatment, but were not detected in the initial treatment UMAP due to subsampling. **D)** (Left) UMAP of the cells that only received combination treatment with dabrafenib and trametinib (Dab/Tram) as an initial treatment. (Right) Venn diagram of clones resistant to each secondary treatment after initial treatment with Dab/Tram. The number of clones that survived multiple secondary treatments are boxed in either blue or red. Cells from these clones are colored on the UMAP (left). The remaining cells are left grey. An arrow indicates a condition where clones were identified as resistant to a second treatment, but were not detected in the initial treatment UMAP due to

subsampling. **E)** (Left) UMAP displaying Dab/Tram to $CoCl_2$ and $CoCl_2$ to Dab/Tram. Cells are colored by treatment condition. (Right) Venn diagram showing that only a single clone was resistant to both sets of treatments. **F)** (Left) UMAP displaying Dab/Tram to cisplatin and cisplatin to Dab/Tram. Cells are colored by treatment condition. (Right) Venn diagram showing that no clones were resistant to both sets of treatments. **G)** (Left) UMAP displaying $CoCl_2$ to cisplatin and cisplatin to $CoCl_2$. Cells are colored by treatment condition. (Right) Venn diagram showing that no clones were resistant to both sets of treatments.

Supplemental Table 1

Primers for amplifying barcodes from gdna	
GHi5.2.1	AATGATACGGCGACCACCGAGATCTACACTAGATCGCACACTCTTTCCCTACACGACGCTCTTCCGATCTNHNNNNTCGACTAAACGCGCTACTTG
GHi5.2.2	AATGATACGGCGACCACCGAGATCTACACCTCTCTATACACTCTTTCCCTACACGACGCTCTTCCGATCTNHNNNNCGTCGACTAAACGCGCTACTTG
GHi5.2.3	AATGATACGGCGACCACCGAGATCTACACTATCCTCTACACTCTTTCCCTACACGACGCTCTTCCGATCTNHNNNNGACTCGACTAAACGCGCTACTTG
GHi5.2.4	AATGATACGGCGACCACCGAGATCTACACAGAGTAGAACACTCTTTCCCTACACGACGCTCTTCCGATCTNHNNNNATAGTCTCGACTAAACGCGCTACTTG
GHi5.2.5	AATGATACGGCGACCACCGAGATCTACACGTAAGCAGACACTCTTTCCCTACACGACGCTCTTCCGATCTNHNNNNTACGTCGACTAAACGCGCTACTTG
GHi5.2.6	AATGATACGGCGACCACCGAGATCTACACACTGCGTAACACTCTTTCCCTACACGACGCTCTTCCGATCTNHNNNNCCTAATCGACTAAACGCGCTACTTG
GHi5.2.7	AATGATACGGCGACCACCGAGATCTACACAAGGAGTAACACTCTTTCCCTACACGACGCTCTTCCGATCTNHNNNNTCGACTAAACGCGCTACTTG
GHi5.2.8	AATGATACGGCGACCACCGAGATCTACACCTAAGCCTACACTCTTTCCCTACACGACGCTCTTCCGATCTNHNNNNGCTCGACTAAACGCGCTACTTG
GHi5.2.9	AATGATACGGCGACCACCGAGATCTACACCGTCTAATACACTCTTTCCCTACACGACGCTCTTCCGATCTNHNNNNCTGTCGACTAAACGCGCTACTTG
GHi5.2.10	AATGATACGGCGACCACCGAGATCTACACTCTCTCCGACACTCTTTCCCTACACGACGCTCTTCCGATCTNHNNNNTATCAGTCGACTAAACGCGCTACTTG
GHi5.2.11	AATGATACGGCGACCACCGAGATCTACACTCGACTAGACACTCTTTCCCTACACGACGCTCTTCCGATCTNHNNNNATGCTCGACTAAACGCGCTACTTG
GHi5.2.12	AATGATACGGCGACCACCGAGATCTACACTTCTAGCTACACTCTTTCCCTACACGACGCTCTTCCGATCTNHNNNNGGATATCGACTAAACGCGCTACTTG
GHi7.2.1	CAAGCAGAAGACGGCATACGAGATTAAGGCGAGTGACTGGAGTTCAGACGTGTGCTCTTCCGATCTGTCCTGCTGGAGTTCGTGAC
GHi7.2.2	CAAGCAGAAGACGGCATACGAGATCGTACTAGGTGACTGGAGTTCAGACGTGTGCTCTTCCGATCTAGGTCCTGCTGGAGTTCGTGAC
GHi7.2.3	CAAGCAGAAGACGGCATACGAGATAGGCAGAAGTGACTGGAGTTCAGACGTGTGCTCTTCCGATCTTCAAGTCCTGCTGGAGTTCGTGAC
GHi7.2.4	CAAGCAGAAGACGGCATACGAGATTCCTGAGCGTGACTGGAGTTCAGACGTGTGCTCTTCCGATCTCACTTAAGTCCTGCTGGAGTTCGTGAC
GHi7.2.5	CAAGCAGAAGACGGCATACGAGATCGACTCCTGTGACTGGAGTTCAGACGTGTGCTCTTCCGATCTTGTCCTGCTGGAGTTCGTGAC
GHi7.2.6	CAAGCAGAAGACGGCATACGAGATTAGGCATGGTGACTGGAGTTCAGACGTGTGCTCTTCCGATCTCTTGAGTCCTGCTGGAGTTCGTGAC
GHi7.2.7	CAAGCAGAAGACGGCATACGAGATATCGCTACGTGACTGGAGTTCAGACGTGTGCTCTTCCGATCTGTAGTCCTGCTGGAGTTCGTGAC
GHi7.2.8	CAAGCAGAAGACGGCATACGAGATCAGAGAGTGTGACTGGAGTTCAGACGTGTGCTCTTCCGATCTGATACTGTCCTGCTGGAGTTCGTGAC

Primers for amplifying barcodes from cdna	
GH_i5.1.1	AATGATACGGCGACCACCGAGATCTACACCTAGCGCTACACTCTTTCCCTACACGACGCTCTTCCGATCT
GH_i5.2.1	AATGATACGGCGACCACCGAGATCTACACTCGATATCACACTCTTTCCCTACACGACGCTCTTCCGATCT
GH_i7.3.1	CAAGCAGAAGACGGCATACGAGATGTCTCTACGTGACTGGAGTTCAGACGTGTGCTCTTCCGATCTAGGACGAGCTGTACAAGTAGG

GH_i7.3.2	CAAGCAGAAGACGGCATACGAGATCAGATAGTGTGACTGGAGTTCAGACGTGTGCTCTT CCGATCTCTGGACGAGCTGTACAAGTAGG
GH_i7.3.3	CAAGCAGAAGACGGCATACGAGATTCTACGCAGTGACTGGAGTTCAGACGTGTGCTCTT CCGATCTTGCGGACGAGCTGTACAAGTAGG
GH_i7.3.4	CAAGCAGAAGACGGCATACGAGATCGACTCTGGTGACTGGAGTTCAGACGTGTGCTCTT CCGATCTGCTCGGACGAGCTGTACAAGTAGG
i7.3.5	CAAGCAGAAGACGGCATACGAGATACGCATTCGTGACTGGAGTTCAGACGTGTGCTCTT CCGATCTGGACGAGCTGTACAAGTAGG
i7.3.6	CAAGCAGAAGACGGCATACGAGATTTCTGAATGTGACTGGAGTTCAGACGTGTGCTCTT CCGATCTAGTACGGACGAGCTGTACAAGTAGG

Supplemental Table 2

Initial cell numbers and growth statistics prior to treatment		
Number of initial barcoded cells counted by hand	**Number of cells on day0 counted by hand**	**Number of doublings by day0**
425000	18412500	5.437078874

Estimated cell numbers and clones sizes entering initial treatment				
Estimated number of cells frozen for barcode sequencing at day0 (1/3 total)	**Number of unique clones detected at day0 and after initial treatments (Union of Fig. 2D and Supp. Fig. 2F)**	**Number of cells going into each initial treatment**	**Estimated average number of cells per clone going into each initial treatment (based on counted number of clones)**	**Estimated average number of cells per clone going into each initial treatment (based on detected clones)**
6137500	60137	4050000	9.529411765	67.34622612
		^ 18 plates at 225,000 cells/plate		
		at day0		
		18287500		

Estimated cell numbers entering secondary treatments							
Initial treatment	**Number of unique clones detected at initial and secondary treatments (Fig. 2D)**	**Number of counted cells after treatment**	**Number of cells frozen for barcode sequencing**	**Number of total wells replated**	**Cells/well replating**	**Number of cells going into each secondary treatment**	**Estimated average number of cells per clone going into each secondary treatment**
trametinib	1350	245125	61281.25	9	20400	61200	45.33333333
CoCl2	895	508800	116070	15	25400	127000	141.8994413
cisplatin	8606	1440000	360000	48	24125	386000	44.85242854